AD-A137 826 DYNAMIC MODELS OF NEURAL SYSTEMS: PROPAGATED SIGNALS PHOTORECEPTOR TRANDD..(U) BOSTON UNIV MA DEPT OF MATHEMATICS S GROSSBERG NOV 83 AFOSR-TR-84-0022 1/2

UNCLASSIFIED AFOSR-82-0148 F/G 6/16 NL

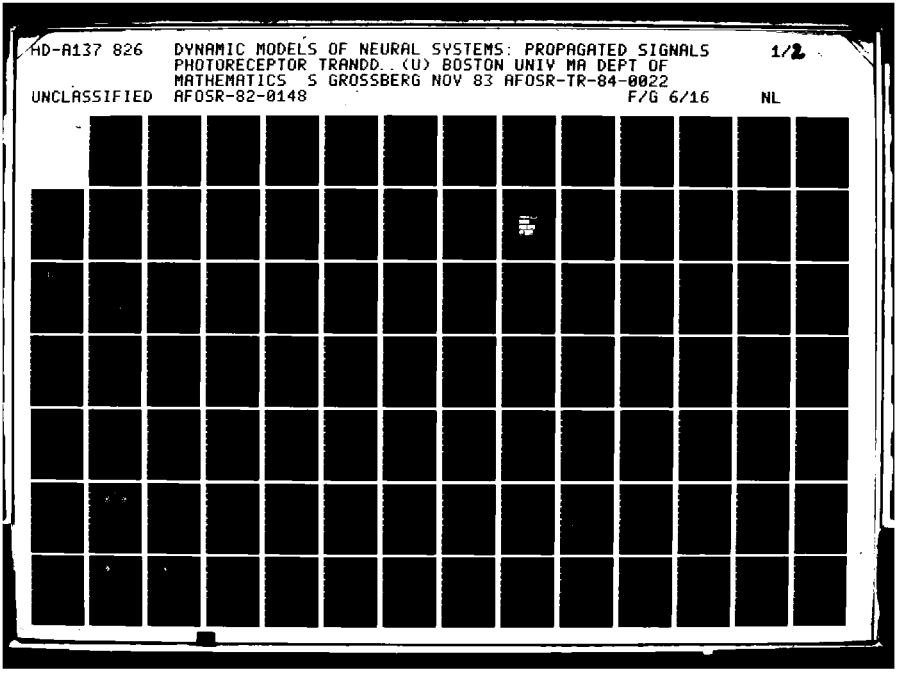

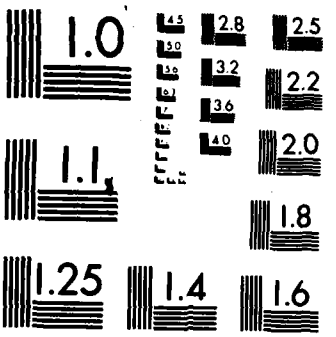

MICROCOPY RESOLUTION TEST CHART
NATIONAL BUREAU OF STANDARDS-1963-A

UNCLASSIFIED

SECURITY CLASSIFICATION OF THIS PAGE (When Data Entered)

REPORT DOCUMENTATION PAGE		READ INSTRUCTIONS BEFORE COMPLETING FORM
1. REPORT NUMBER AFOSR-TR- 84 0022	2. GOVT ACCESSION NO.	3. RECIPIENT'S CATALOG NUMBER
4. TITLE (and Subtitle) DYNAMIC MODELS OF NEURAL SYSTEMS: PROPAGATED SIGNALS, PHOTORECEPTOR TRANSDUCTION, AND CIRCADIAN RHYTHMS		5. TYPE OF REPORT & PERIOD COVERED Final Report 6. PERFORMING ORG. REPORT NUMBER
7. AUTHOR(s) Dr. Stephen Grossberg		8. CONTRACT OR GRANT NUMBER(s) AFOSR-82-0148
9. PERFORMING ORGANIZATION NAME AND ADDRESS Department of Mathematics Boston University Boston, MA 02215		10. PROGRAM ELEMENT, PROJECT, TASK AREA & WORK UNIT NUMBERS 2313/A5 61102F
11. CONTROLLING OFFICE NAME AND ADDRESS Air Force Office of Scientific Research/NL Bolling AFB, DC 20332		12. REPORT DATE November 1983 13. NUMBER OF PAGES 96
14. MONITORING AGENCY NAME & ADDRESS(if different from Controlling Office)		15. SECURITY CLASS. (of this report) UNCLASSIFIED 15a. DECLASSIFICATION/DOWNGRADING SCHEDULE

16. DISTRIBUTION STATEMENT (of this Report)

Approved for public release;
distribution unlimited.

17. DISTRIBUTION STATEMENT (of the abstract entered in Block 20, if different from Report)

ELECTE
FEB 1 0 1984
A

18. SUPPLEMENTARY NOTES

19. KEY WORDS (Continue on reverse side if necessary and identify by block number)

Bionocular Phenomena, Chemical Transmitters, Parameters

20. ABSTRACT (Continue on reverse side if necessary and identify by block number)

Three concepts are used to illustrate how a small number of simple mechanisms can generate a wide diversity of complex biological phenomena, as well as parametric experimental tests of the models that simulate these phenomena. One is the classical concept that a membrane equation can model fast electrical responses in cells. The second is the concept that mass action processes can be coupled to the membrane equation as conductance terms. The third is the concept that gating processes can be used to model the mass action dynamics of chemical transmitters.

DD FORM 1 JAN 73 1473 EDITION OF 1 NOV 65 IS OBSOLETE

UNCLASSIFIED

SECURITY CLASSIFICATION OF THIS PAGE (When Data Entered)

AFOSR-TR- 84-0022

Final Scientific Report
AFOSR-82-0148
November 1983

DYNAMIC MODELS OF NEURAL SYSTEMS: PROPAGATED SIGNALS, PHOTORECEPTOR TRANSDUCTION, AND CIRCADIAN RHYTHMS

Boston University
Department of Mathematics
Boston, MA 02215

Dr. Stephen Grossberg

Controlling Office: Air Force Office of Scientific Research/NL
Bolling Air Force Base, DC 20332

TABLE OF CONTENTS

TABLE OF CONTENTS (cont.)

INTRODUCTION

This article presents dynamical system models of three types of related neural phenomena: electrical signal patterns in individual nerves, transduction of light into electrical signals by photoreceptors, and the electrical, chemical, and light interactions that control circadian rhythms.

Each of these phenomena takes place in a complex neural system, which can be experimentally analyzed by a variety of techniques, each technique probing different levels of system organization; e.g., behavioral, neurophysiological, anatomical, and molecular. Our modelling approach aims to discover and to classify system properties that will persist as new experimental methods are developed. To achieve this goal, each model mechanizes basic principles of neural design which we suggest are rate-limiting in the data gathered by any of several methods. To test whether these principles are operative in the cases we discuss, each model is used to predict how several data indices will simultaneously vary in response to prescribed parameter changes in each model. These predictions should hold not only in the cases treated herein, but also in all neural systems where these principles are rate-limiting. The predictions are in this sense general invariants that can be sought in any body of neural data.

In this spirit, we examine detailed parametric properties of solutions of differential equation models, both analytically and numerically, and compare these properties with related data. By contrast, various other approaches have sought the existence of solutions to justify a model, but have not discussed the detailed parametric structure of these solutions. For example, there has recently been great interest in the complex dynamics which can arise in such simple systems as maps of the interval (Feigenbaum, 1978; Li and Yorke, 1975). The combination of simple equations and complex dynamics has made

these systems appealing candidates for biological models (Guevara et al, 1981; May, 1976). Our models are also capable of generating complex, even chaotic waveforms, but we believe that the predictable parametric regularities of the model solutions provide the strongest argument for their physical relevance.

I. SIGNAL PATTERNS IN SINGLE NERVE CELLS

I.1. Parametric Classification of Signal Patterns

In this section we examine a class of dynamical systems that generalizes the famous Hodgkin-Huxley (1952) model of nerve impulse propagation. Despite the many variations that exist across nerve cells and, more generally, excitable membranes throughout phylogeny, the intuitive concepts of ionic interactions with membrane voltage that led to the Hodgkin-Huxley (1952) model have proved to be universal. The generalized Hodgkin-Huxley model attempts to rigorously capture both the invariant intuition and the many variations on the ionic hypothesis. To structure some of these experimental variations and to test whether Hodgkin-Huxley dynamics generate the observed signal patterns, the detailed parametric properties of model solutions have been examined and classified (Carpenter, 1977a, 1977b, 1979, 1981).

One surprising result of this analysis is that the mere existence of the elementary components of impulse propagation (Na^+ entering the cell followed by K^+ leaving the cell) implies many properties which had previously been ascribed to additional membrane processes. For example, bursting patterns measured from epileptic neurons have been ascribed to a complex interaction between neurons (Ward, 1969), but these bursting patterns can be generated by individual neurons (Carpenter, 1979, 1981). Other characteristics of the data had not even

been noticed. For example, there exist two types of regular periodic (beating) signal patterns, each type possessing a series of correlated distinguishing properties. The model hereby structures signal patterns that had previously seemed to be so irregular that their fine structure was ignored. In this sense, the model helps to define what the reliable data properties are by parametrically relating these properties to a single underlying mechanism.

In this article, a number of parametric model predictions will be presented. It is important to emphasize what we mean by a prediction. A prediction is a property of the model in question. If one of these properties fails to hold in vivo, either the model is inapplicable or there are additional factors at work. We will consider examples of data which do not correspond to the predicted solution types of one Hodgkin-Huxley model, but do correspond to the predicted solution types of a related Hodgkin-Huxley model that possesses one more ionic process. An important goal of the classification theory is to discover the minimal number and type of ionic processes that are needed to generate prescribed signal patterns. From this perspective, the popular FitzHugh-Nagumo model (Evans, Fenischel, and Feroe, 1982; FitzHugh, 1961; Hastings, 1982; McKean, 1970; Nagumo, Arimoto, and Yoshizawa, 1962; Rinzel and Keller, 1973) is a variant of a generalized Hodgkin-Huxley model with one ionic process less than the original Hodgkin-Huxley (1952) model.

I.2. The Hodgkin-Huxley Equations

The original Hodgkin-Huxley (1952) model was derived from experimental studies of the squid giant axon. The axon of a nerve cell is a long cylindrical process that leads from the nerve cell body to other cells or muscles (Figure 1). Propagated signals can hereby be transmitted along axons between communicating cells. The Hodgkin-Huxley

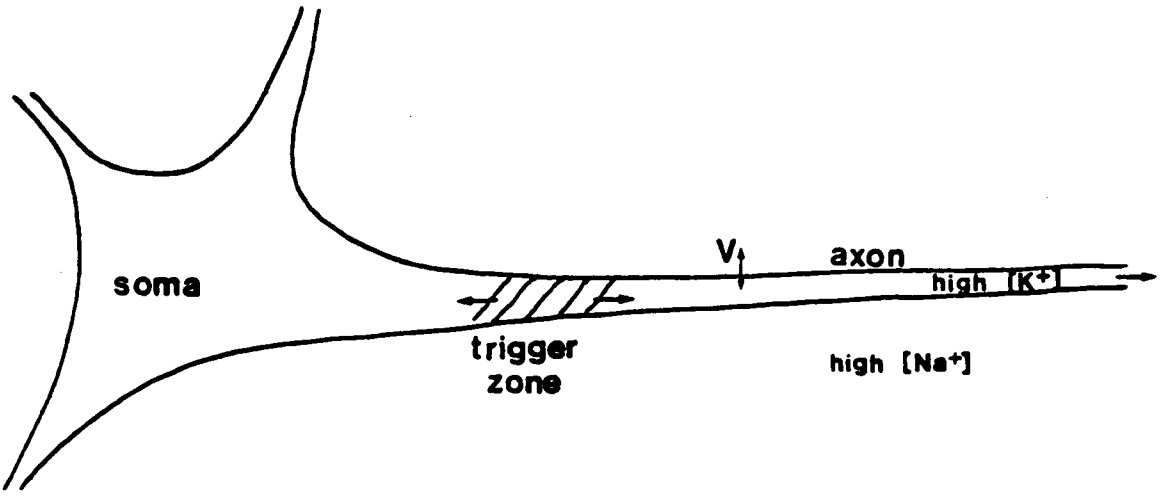

Figure 1: Schematic view of part of a nerve cell.

model describes interactions between membrane voltage V and three ionic variables m, n, and h capable of generating these propagated signals.

Denoting the distance traveled from the nerve cell body down the axon by the variable x, the Hodgkin-Huxley (1952) equations describe how the ionic processes m(x,t), n(x,t), and h(x,t) interact with the voltage V(x,t) at each position x and time t, and how the voltages at nearby positions influence each other via diffusion. The equation governing the voltage V(x,t) is the membrane equation

$$\frac{a}{2R}\frac{\partial^2 V}{\partial x^2} = C\frac{\partial V}{\partial t} + g(V,m,n,h) \qquad (1)$$

where the term $\frac{a}{2R}\frac{\partial^2 V}{\partial x^2}$ is the total membrane current density (by Ohm's law) and the term $C\frac{\partial V}{\partial t}$ is the capacitance current density. These two

terms control the diffusion of voltage between spatial positions. The remaining term g(V,m,n,h) is the total ionic current density, which is defined by Hodgkin and Huxley (1952) as

$$g(V,m,n,h) = \bar{g}_{Na}m^3h(V-V_{Na}) + \bar{g}_K n^4(V-V_K) + \bar{g}_L(V-V_L). \qquad (2)$$

Each summand in (2) is a product of a conductance times a voltage difference. Term $\bar{g}_{Na}m^3h(V-V_{Na})$ is the (inward) sodium current density; term $\bar{g}_K n^4(V-V_K)$ is the (outward) potassium current density; and $\bar{g}_L(V-V_L)$ is a leakage current density. The main step in generalizing the Hodgkin-Huxley equations is to consider total ionic currents more general in form than (2) that may include fewer or more ionic currents, and to characterize the qualitative properties of those functions that control signal properties.

The voltage is coupled to the ionic processes via equations of the form

$$\frac{\partial m}{\partial t} = \gamma_m(V)\,(m_\infty(V)-m) \qquad (3)$$

$$\frac{\partial n}{\partial t} = \gamma_n(V)\,(n_\infty(V)-n) \qquad (4)$$

and

$$\frac{\partial h}{\partial t} = \gamma_h(V)\,(h_\infty(V)-h). \qquad (5)$$

Each of the ionic equations is of the same general form. Equation (3), for example, possesses a positive voltage-dependent rate term $\gamma_m(V)$ and a positive voltage-dependent asymptote $m_\infty(V)$ to which m is attracted. The ionic equations differ in two basic ways. Some ionic processes respond quickly to voltage changes, others slowly. Some ionic processes increase with voltage increments, others decrease. Since m responds quickly relative to n and h, $\gamma_m(V)$ is large relative to $\gamma_n(V)$ and $\gamma_h(V)$. Since m and n tend to increase whereas h tends to decrease

as V increases, $m_\infty(V)$ and $n_\infty(V)$ are increasing functions of V whereas $h_\infty(V)$ is a decreasing function of V. The choice of fast-slow and on-off distinctions are characteristic of the qualitative hypotheses that define the class of generalized Hodgkin-Huxley models and distinguish one model from another.

I.3. Propagated Signals and Traveling Waves

To study signals propagated along an axon, solutions are sought of the form

$$V(x,t) = V(s) \tag{6}$$

where

$$s = x + \omega t. \tag{7}$$

In other words, one seeks solutions which propagate down the axon (x) through time (t) at a speed (ω). Such solutions are called traveling waves. When (6) holds, equation (1) can be rewritten as the pair of equations

$$\frac{dV}{ds} = W \tag{8}$$

and

$$\frac{dW}{ds} = \epsilon W + g(V,m,n,h) \tag{9}$$

in terms of the new independent variable s and the parameter

$$\epsilon = \frac{2RC\omega}{a} . \tag{10}$$

To emphasize the fact that m responds quickly whereas n and h respond slowly to fluctuations in V, we can redefine the voltage-dependent rate functions and rewrite equations (3)-(5) in terms of the new independent variable s as

$$\frac{dm}{ds} = \varepsilon^{-1}\gamma_m(V)\,(m_\infty(V)-m) \tag{11}$$

$$\frac{dn}{ds} = \varepsilon\gamma_n(V)\,(n_\infty(V)-n) \tag{12}$$

and

$$\frac{dh}{ds} = \varepsilon\gamma_h(V)\,(h_\infty(V)-h)\,. \tag{13}$$

Since both ε and ε are assumed to be small, the rate function $\varepsilon^{-1}\gamma_m(V)$ is large compared to the rate functions $\varepsilon\gamma_n(V)$ and $\varepsilon\gamma_h(V)$.

I.4. Bursts and Two Types of Regular Periodic Waves: Predictions and Data

Previous articles have developed the mathematical analysis of system (8)-(13) (Carpenter, 1977a,b, 1979, 1981). Here, we will focus on the detailed predictions of that analysis; compare the predicted solutions with experimental recordings; examine some types of signal patterns which are not consequences of the basic sodium-potassium mechanisms; and consider ways in which the model may be augmented to account for these patterns.

First we will consider experimental and mathematical evidence for the existence of two types of regular periodic waveforms and how these are related to periodic bursts. Examples of these signal patterns can be seen in Figure 2, which shows recordings taken from two snail yellow cells (Benjamin, 1978). Each column in Figure 2 depicts signal patterns measured in a single cell. Each signal pattern in a given column occurs when the cell is maintained at a given level of hyperpolarization, which is denoted by i. Both cells emit regular periodic signals when i=0, as in the bottom row of Figure 2, but cell A has a higher frequency. As the cells are gradually hyperpolarized (i becomes negative), cell A moves through a region of high frequency

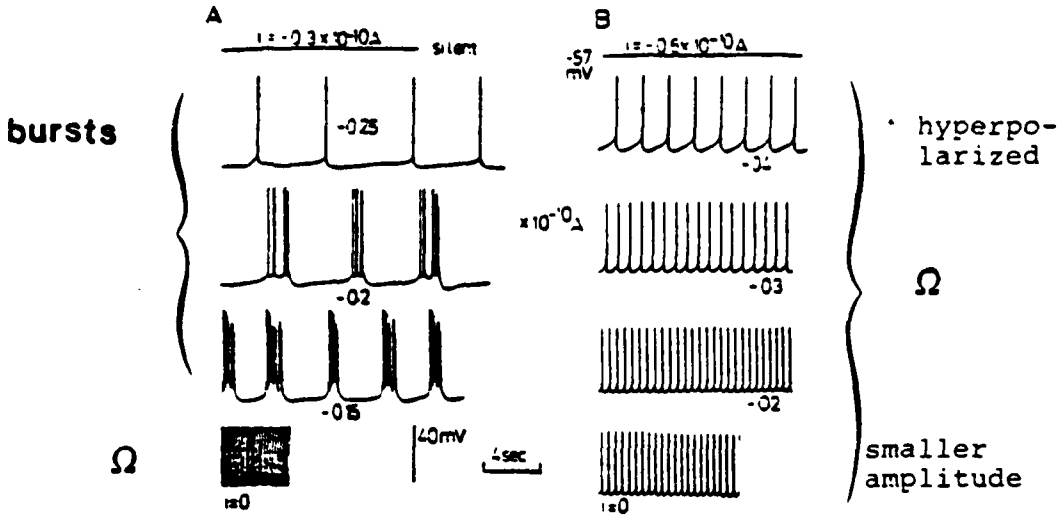

Figure 2: Recordings from two similar snail yellow cells (Benjamin, 1978, p.208), which illustrate the two types of predicted dynamics of the generalized Hodgkin-Huxley model. From bottom to top, cells are hyperpolarized until they become silent. (A) High frequency Ω-periodic spikes (i=0) pass through a phase of bursts with many spikes, then bursts with few spikes, then 1-bursts, then silent: exactly as predicted. (B) In a cell without bursts (the other "half") high frequency Ω-periodics become low frequency Ω-periodics, then silent.

bursts, then low frequency bursts, then low frequency beats, then becomes silent. Cell B continues to emit regular periodic signals whose frequency declines gradually as i becomes negative until it, too, is silent. Previous theorems (Carpenter, 1979, 1981) not only predict the existence of the two types of signal patterns observed in cells A and B, but also lead to further predictions, which cells A and B confirm on closer inspection. Some of these predictions follow.

The most obvious difference between cells A and B in Figure 2 is that cell A emits burst patterns at certain levels of hyperpolarization, but cell B never bursts. Until recently, it was not known that Hodgkin-Huxley dynamics could lead to bursts at all. Surprisingly, it

has been proved that "half" of all generalized Hodgkin-Huxley models, in a sense that can be made precise, admit bursting solutions (Carpenter, 1979). Given the unexpected ease with which bursts can be generated, it is imperative to study the detailed internal structure of these bursts to ascertain their underlying mechanism. It was also proved that all generalized Hodgkin-Huxley models admit regular periodic solutions, as do both cells A and B in Figure 2. To emphasize the meaning of these general results on bursts and periodic solutions, we mention that snail yellow cells, as in Figure 2, may sustain bursts in one season but only regular periodic patterns in another season (Benjamin, 1978). This can be explained by a suitable parameter shift in a generalized Hodgkin-Huxley model that removes the model from the parameter range where bursts occur to the parameter range where only regular periodic solutions occur.

The analysis of burst solutions leads to a geometric understanding of the phase portrait which is illustrated schematically in Figure 3. In Figure 3A, a burst with many spikes per burst, a so-called N-burst with $N >> 1$, is depicted. Each loop in the bursting trajectory corresponds to one spike in the cell's potential, as in Figure 2A. As more spikes in a burst unfold, the N-burst trajectory approaches a regular periodic solution that lies far from the equilibrium point (rest) in phase space. The regular periodic solution is called an <u>Ω-periodic</u> solution. When N is large, spikes late in the burst are all but indistinguishable from spikes in the Ω-periodic solution. Thus late in the burst, it appears as if the trajectory is approaching a limiting (ω-limit) set which in this case is the Ω-periodic solution. The part of the N-burst trajectory denoted by Q is a quiet spell during which the cell potential approaches close to equilibrium before the bursting cycle begins again.

The fact that an N-burst starts near rest and ends near an Ω-

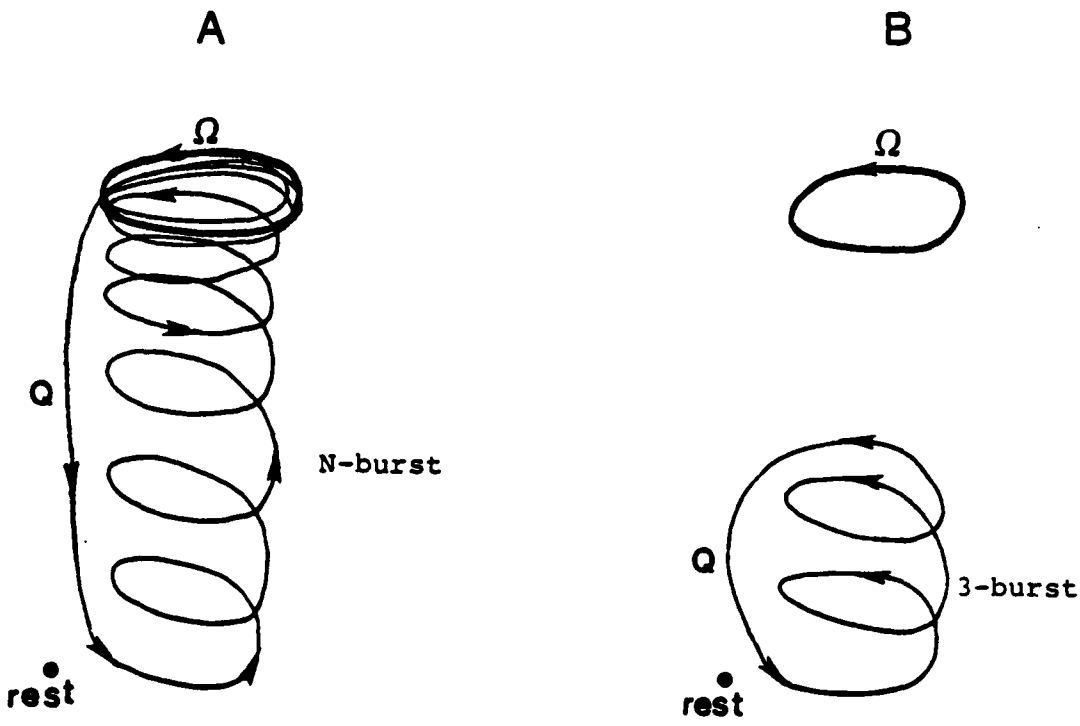

Figure 3: Schematic representation, in phase space, of Ω-periodic solutions and (A) a burst with N spikes per burst; and (B) a burst with 3 spikes per burst. During the quiet spell (Ω) the burst solutions approach the rest point.

periodic solution far from rest has important implications for the internal structure of each burst. Spikes emitted close to rest will be emitted at a slow rate whereas spikes emitted close to the Ω-periodic solution far from rest will form a high frequency pattern of approximately equally spaced spikes. Thus the spikes within a burst will speed up until they abruptly shut off.

Figure 3B depicts a 3-burst. Since the last spike in this burst is far from the Ω-periodic solution, all the spikes are emitted at a lower rate than the final spikes in the N-burst of Figure 3A. Since no spike in the 3-burst is close to the Ω-periodic solution, the regular frequency which the Ω-periodic solution imposes on the final

spikes in the N-burst need not appear in the 3-burst. Finally, compare the quiet spells Q in the N-burst of Figure 3A and the 3-burst of Figure 3B. Although both quiet spells correspond to a narrow range of subthreshold cell potentials, Figure 3 shows that they actually correspond to rather different paths in phase space. Consequently the durations of quiet spells between bursts with different numbers of spikes need not be the same. This point will be illustrated in Figure 9 below.

A generalized Hodgkin-Huxley model that possesses an N-burst solution also possesses a 1-burst, 2-burst, 3-burst,....., and an (N-1)-burst solution (Carpenter, 1979). Consequently, every generalized Hodgkin-Huxley model that admits bursts at all will admit 1-burst solutions. A 1-burst solution is a regular periodic solution (Figure 4). However, <u>all</u> generalized Hodgkin-Huxley models admit Ω-periodic

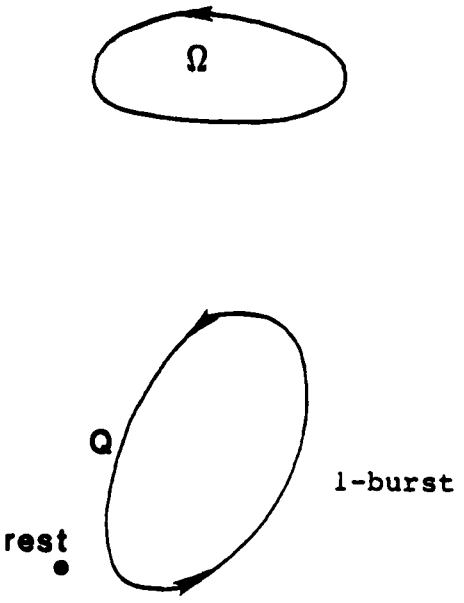

Figure 4: Schematic representation of the two types of regular periodic solutions whose existence is predicted in the "half" of the model cells which burst. The Ω-periodic is far from equilibrium while the 1-burst approaches equilibrium during the quiet spell.

solutions, which are also regular periodic solutions. Thus "half" of all generalized Hodgkin-Huxley models admit two classes of mechanistically distinct regular periodic solutions. How can an experimentalist know which regular periodic solution is being seen when a cell emits periodic spikes? To answer this question, the following parametric properties of each type of regular periodic solution may prove helpful.

First, in a model cell capable of bursting, the family of Ω-periodic solutions is always far from equilibrium, while each solution in the co-existing family of 1-burst solutions always approaches equilibrium during its quiet spell. Thus, we would expect that a small hyperpolarization of cell potential during a periodic 1-burst could easily extinguish this pattern, but a much larger hyperpolarization would be required to extinguish an Ω-periodic. Moreover, if an Ω-periodic pattern is hyperpolarized, it can become an N-burst solution. Given larger hyperpolarizations, N will tend to decrease. Given a large enough hyperpolarization, the Ω-periodic can be extinguished.

This prediction corresponds exactly to what occurs in Figure 2A, where successively larger hyperpolarizations transform a regular periodic pattern into bursting patterns with progressively fewer spikes per burst.

In generalized Hodgkin-Huxley models wherein bursts do not occur (the other "half" of the models), the regular periodic solutions that do occur are all Ω-periodic solutions. Hyperpolarization of such a solution moves it closer to rest, and thereby decreases the frequency of its spikes. If the hyperpolarization is chosen sufficiently large, the Ω-periodic solution is extinguished.

Figure 2B nicely illustrates this prediction. Successively greater hyperpolarizations cause progressively lower spiking frequencies, but do not cause bursts to occur, by contrast with Figure 2A.

Notice that the individual waveforms in Figure 2 differ in several ways which are hard to categorize a priori. For example, the waveforms corresponding to low frequency patterns in row 1 of the Figure are different. The periodic patterns of different frequency within column 1 and within column 2 of the Figure are different. Below, several of these differences will be parametrically characterized as typical predictions of Hodgkin-Huxley dynamics. It will also be shown how a single family of solutions in a model capable of bursting can possess properties from both column 1 and column 2 in a predictable order.

Because the underlying parameters of a given cell are not known a priori, the most robust predictions arise when the cell is parametrically perturbed in an experimentally controlled way, as in Figure 2A or 2B. Nonetheless it may be noted, as in row 1, that low frequency 1-periodic solutions possess a strictly increasing ramp-like potential between successive spikes, whereas low frequency 1-bursts tend to be flat over a significant fraction of the interspike interval. Figure 2B illustrates the fact that 1-periodic solutions of higher frequency tend to have smaller spike amplitudes. By contrast, the spike amplitudes of all bursts in Figure 2A are approximately constant in size. Finally, the spike amplitudes of all bursts exceed the spike amplitudes of high-frequency 1-periodic solutions in a given model cell. In fact, the spike amplitudes of the 1-bursts in row 1 of Figure 2A are 50% larger than the amplitudes of the 1-periodic spikes in row 4 of Figure 2A. These qualitative remarks are made more quantitative in the set of predictions depicted by Figures 5 and 6 below.

I.3. A Single Family of 1-Bursts and 1-Periodic Wave Trains

A family of 1-bursts, as in Figure 2A, and a family of 1-periodic solutions, as in Figure 2B, may or may not meet in phase space as

changes in initial data generate successive members of the family (Carpenter, 1979). Figure 5 depicts a family of solutions where the

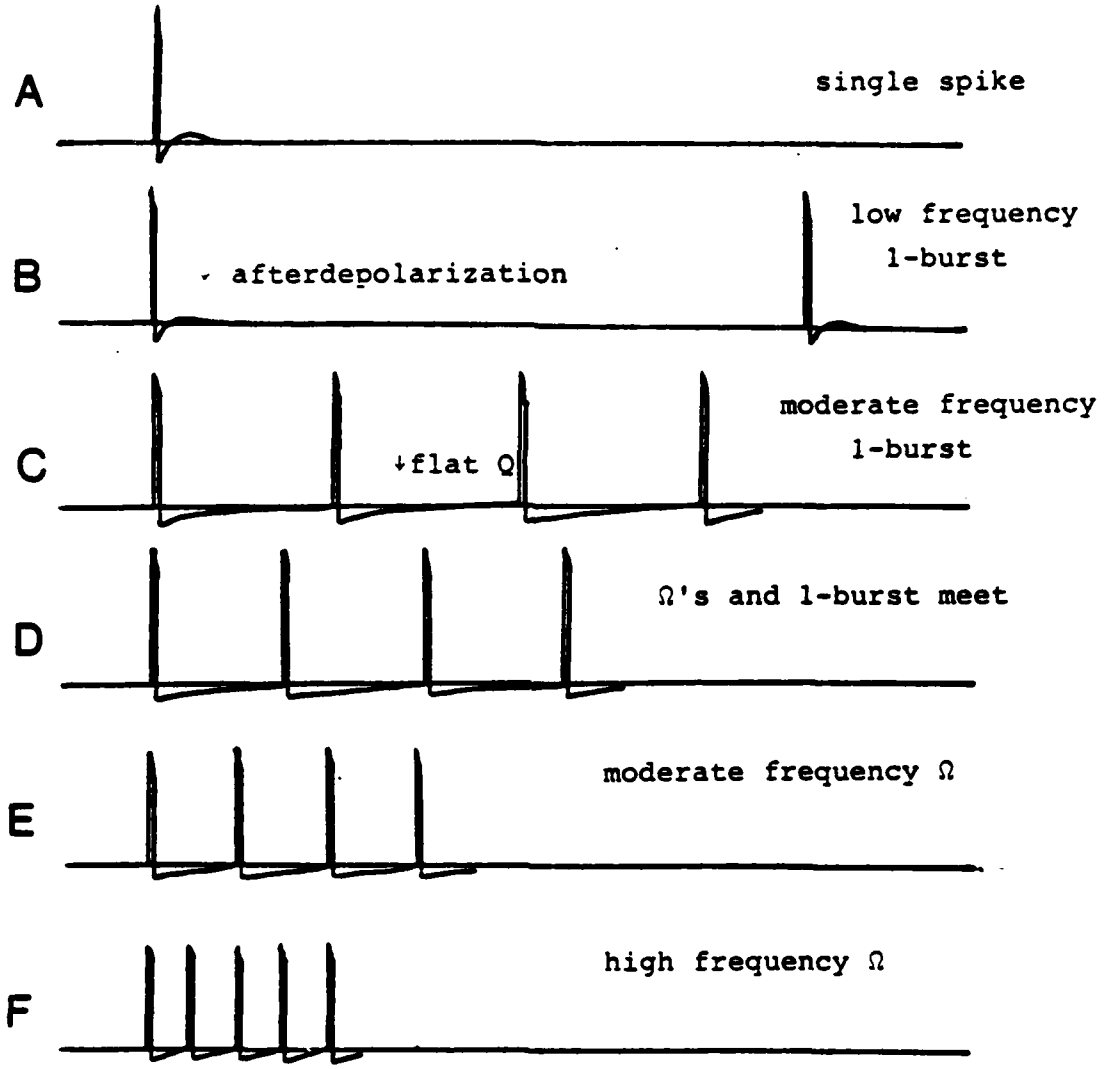

Figure 5: A typical family of regular periodic solutions of a generalized Hodgkin-Huxley model which has burst solutions. In this example, the 1-burst family and the Ω-periodic family meet, although this need not be the case. The quiet spell goes from ∞ at the single pulse (A) to 0 at the dividing point (D). The 1-burst frequencies range from very low to moderate and the Ω-periodic frequencies range from moderate to very high. The amplitudes of the 1-bursts ((A)-(D)) are large and approximately constant over their wide frequency range. In contrast, the amplitudes of the Ω-periodics decline as the frequency increases, as does the size of the hyperpolarization, or tail, following each spike.

two types of regular periodic patterns do meet. Figure 5A depicts a single spike, whose potential goes to the rest point both as $t \to +\infty$ and as $t \to -\infty$. Nearby in phase space is a 1-burst periodic solution (Figure 5B), which comes very close to the rest point during its quiet spells Q and thus has a low frequency. Such a low frequency 1-burst may or may not be followed by a brief afterdepolarization (arrow; also see Figure 8B). As the family is perturbed away from the rest point, the frequency decreases to a moderate level as Q shortens (Figure 5C), and the afterdepolarization disappears. As noted in Figure 2A, 1-bursts are relatively flat during their quiet spells Q. The spike amplitude is large and nearly constant over a wide range of frequencies.

In Figure 5, high frequency 1-bursts join a family of Ω-periodic solutions. At the meeting point the frequency is moderate. Moving into the family of Ω-periodics (Figure 5E), the frequency increases further. As noted in Figure 2B, activity steadily increases throughout the interspike interval. The Ω-periodic family terminates at very high frequency (Figures 5F and 2A). High frequency Ω-periodic solutions have significantly smaller spikes than do low frequency Ω-periodic solutions, by contrast with 1-bursts.

I.6. Fine Structure of Ω-Periodic Waves

Figure 6 illustrates some detailed predictions of the generalized Hodgkin-Huxley model. These predictions describe the covariation of several properties of Ω-periodic solutions that apply to all model cells, whether or not they admit bursts. If a change of initial data causes a higher frequency of Ω-periodic spikes, then it also causes a lower amplitude of spikes, a smaller post-spike hyperpolarization, a lower wave speed, and a lower spiking threshold. In Figure 2B, the frequency, amplitude, and post-spike hyperpolarization of snail yel-

low cell spikes all covary as predicted, thereby strengthening our contention that Figure 2B illustrates a family of Ω-periodic solutions.

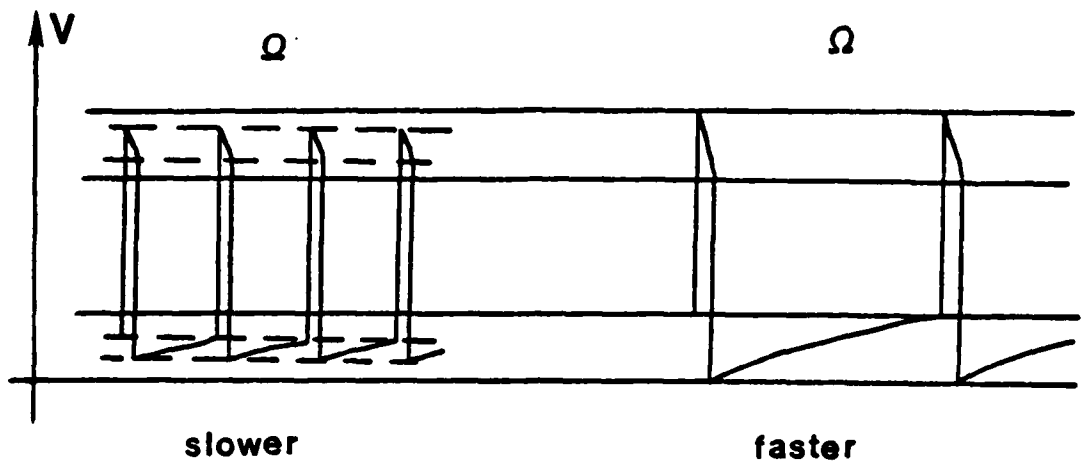

Figure 6: Correlated properties of Ω-periodic solutions

higher frequency	lower frequency
lower amplitude	higher amplitude
smaller post-spike hyperpolarization	larger post-spike hyperpolarization
low speed	moderate or high speed
lower threshold	higher threshold

I.7. Effects of Drugs on Signal Patterns: The Inverse Problem

Another type of data that illustrate these predictions are drug effects on nerve cell signal patterns. A drug may cause complex chemical reactions in many intracellular and intercellular subsystems. Most if not all of these reactions cannot be directly observed. The present approach suggests a new method to help classify which of these reactions are due to intracellular changes, notably changes in the parameters of a Hodgkin-Huxley mechanism, and to generate inferences about which intracellular parameters may have changed. The

method studies the observable parametric changes in a cell's electrical signal patterns and uses these changes to make inferences about corresponding changes in unobservable cell parameters. The attempt to infer underlying mechanisms from observable properties is often called an inverse problem.

Figure 7 depicts a drug effect on a giant neuron of the snail Helix pomatia (Lábos and Láng, 1978) that can be interpreted in terms of our parametric predictions about bursts and Ω-periodic waves. Figure 7A illustrates the regular periodic output of a giant neuron in an

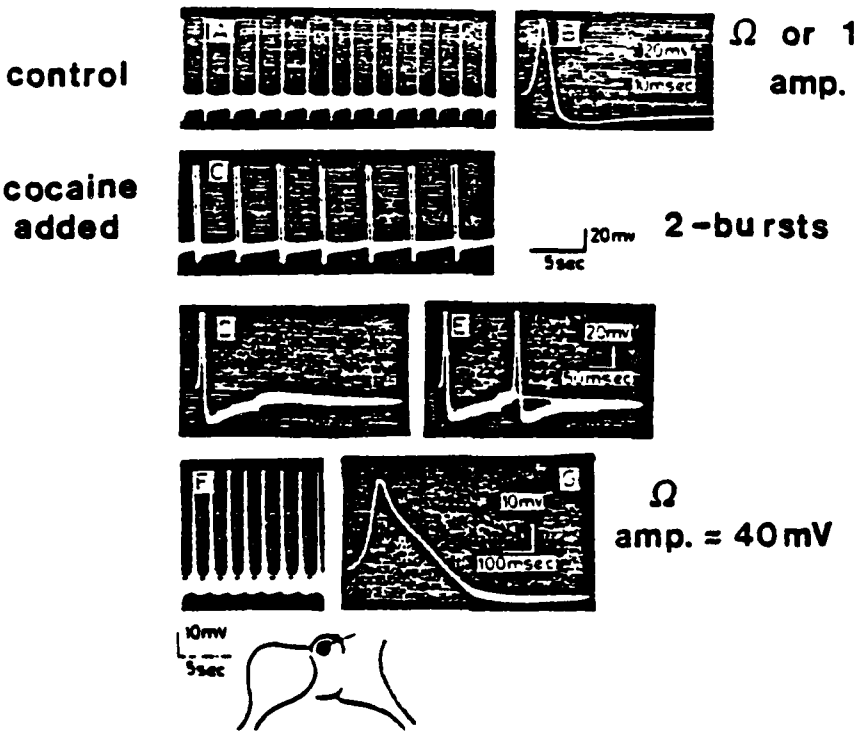

Figure 7: Recordings from snail (Helix) neuron. (A)-(B): control; (C)-(E): 10-25 minutes after administration of cocaine; (F)-(G): after 30 minutes (Lábos and Láng, 1978, p.179). Compare (A) with (F): in (A) the frequency is lower, the amplitude is higher, and the post-spike hyperpolarization is larger - all as predicted in Figure 6.

isolated subesophageal ganglion before cocaine was applied to the bathing fluid. This regular periodic solution is either a periodic 1-burst or an Ω-periodic solution. Recall from Figure 5 that periodic 1-bursts can merge with Ω-periodics in a single family of solutions, so no single picture can tell them apart.

During the first 30 minutes after the cocaine was applied, the regular periodic solution was transformed into a periodic 2-burst solution (Figure 7C). After the first 30 minutes, the effects of the drug started to wear off, leading to the regular periodic solution of Figure 7F, before this solution approached the original waveform in Figure 7A. Despite the incomplete nature of these data for solving the inverse problem, a comparison of Figures 7A and 7F is informative in the light of Figure 6. Figure 6 suggests that Figure 7F depicts an Ω-periodic solution, not a periodic 1-burst. Note that the amplitude of spikes is larger, the frequency of spikes is lower, and the post-spike hyperpolarization is greater in Figure 7A than in Figure 7F, just as predicted in Figure 6. To draw a more complete portrait of underlying cellular changes, a parametric series of dose-dependent waveforms at a regular succession of times after dose would be most helpful.

I.8. Parametric Structure of Bursts

Just as with 1-bursts and Ω-periodics, a series of predictions can be made about N-bursts. The family of all such N-bursts will be called HH bursts to distinguish them from other burst types, such as the parabolic bursts and paroxysmal bursts that occur in data and the FN bursts that are solutions of the FitzHugh-Nagumo model. These other burst types will be discussed later.

As shown in Figure 3A, an HH burst with many spikes per burst moves away from the rest point towards an Ω-periodic solution. Hence its spiking frequency speeds up and becomes more constant late in the

burst. As with 1-bursts, the potential in such an HH burst is nearly flat during the quiet spell Q. Figure 8A contains a periodic bursting solution that illustrates these predictions. This record depicts spon-

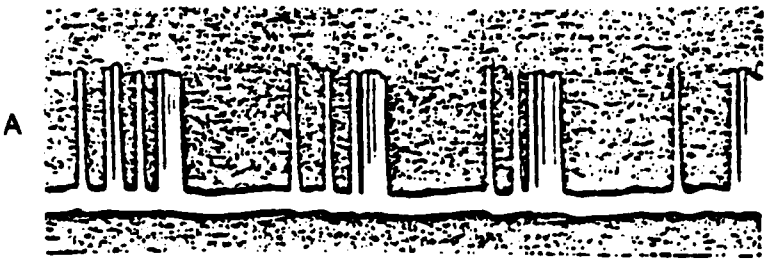

Spontaneous action potentials in monkey epileptic cortex (Atkinson and Ward, 1964, p.291).

Bursts in the lobster stomatogastric ganglion (Russell and Hartline, 1978, p.454).

Bursts in the motor neuron controlling expiration in the dragonfly (Mill, 1977, p.193).

Figure 8: Typical HH burst patterns in intracellular recordings. Note the increasing frequency within the burst; the flat interburst interval; and the afterdepolarization in (B).

taneous action potentials that were recorded from the monkey epileptic cortex (Atkinson and Ward, 1964, p.291). Figure 8C depicts bursts of similar form that were recorded from a motor neuron which controls expiration in the dragonfly (Mill, 1977, p.193). In both figures, the

frequency of spikes increases and levels off before the burst suddenly terminates. Figure 8B depicts a bursting solution with so few spikes per burst that the frequency never speeds up, as also occurs in Figure 3B.

Another prediction for HH bursts is that the length of the quiet spell Q between bursts increases with the number of spikes in each burst, as illustrated in Figure 9 within snail yellow cells. Due to this property, there is a tendency for a fixed number of spikes to occur within a sufficiently long time interval whether these spikes are

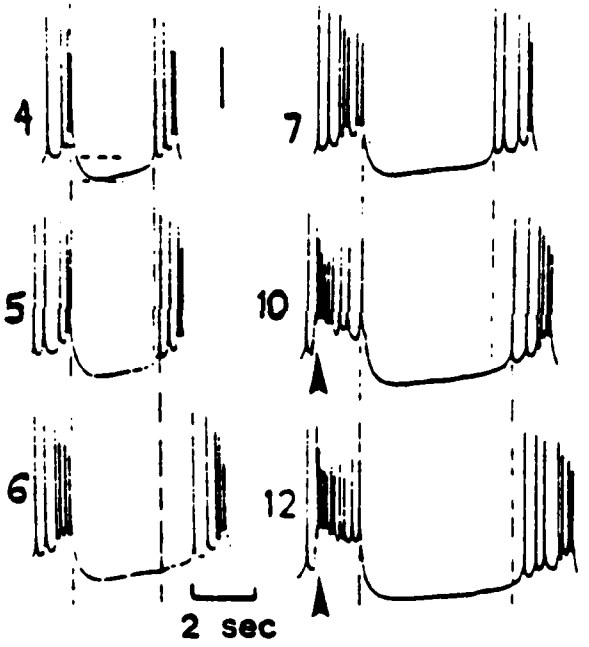

Figure 9: As predicted, the length of the quiet spell increases with the number of spikes in the previous burst in snail (Lymnae stagnalis) yellow cells (Benjamin, 1978, p.209).

grouped into 1-bursts, 2-bursts, and so on. This tendency is illustrated in Figures 7A and 7C. There the application of cocaine resulted in the clustering of spikes into 2-burst doublets, but the average frequency remained the same: each trace has 14 spikes within approximate-

ly 34 seconds.

Even in cells wherein the average spiking frequency remains entirely invariant when the bursts change their structure, these changes can significantly alter the firing of the cells which receive the bursts (Calvin, 1972). This is because a large number of rapidly occurring spikes within a burst can drive the target cell potential to a much higher asymptote than the same number of spikes spread more thinly through time, as Figure 10 schematically illustrates. Carpenter (1979, 1981) makes other predictions concerning the structure of HH bursts, notably their stability under noisy perturbations.

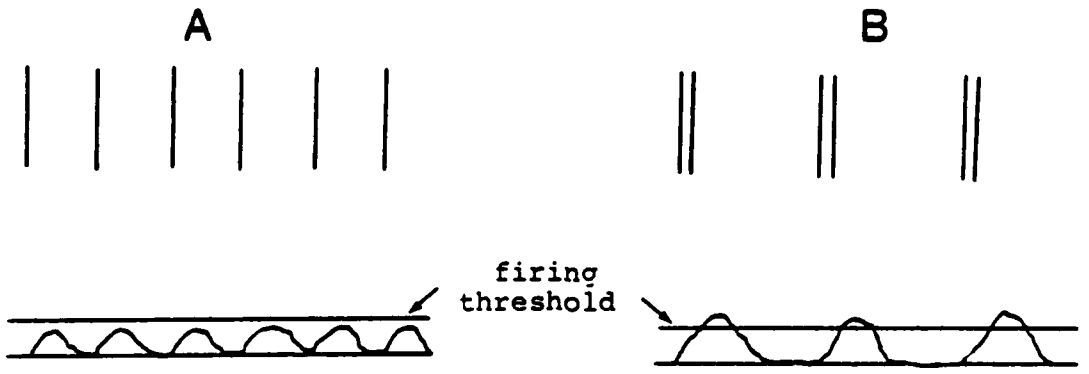

Figure 10: Top row: pre-synaptic spike train. Bottom row: post synaptic transmitter concentration. In (A) and (B), the average spike frequencies are identical. However, the cell which bursts (B) is more excitable than the cell (A) with a regular spike pattern.

I.9. Finite Wave Trains and Chaotic Waveforms: Aperiodic Phenomena

In addition to the periodic bursts and Ω-periodic solutions, several classes of aperiodic waveforms that were not previously known to be consequences of Hodgkin-Huxley dynamics have been mathematically proved to exist (Carpenter, 1977a, 1977b, 1979, 1981).

The simplest aperiodic waveforms are the finite wave trains. These solutions generalize the single spike in Figure 5A. They contain a single burst, preceded and followed by subthreshold activity, whose internal structure is akin to the bursts that occur within periodic bursting solutions. It has been proved that the speed with which such an N-burst travels down the axon is an increasing function of N.

More complex aperiodic waveforms can also exist. Under special hypotheses, all possible sequences of bursts can be generated within a single model neuron. In other words, some model neurons can support an infinite dimensional temporal code despite the fact that they are defined by a five-dimensional dynamical system. More precisely, within such a system, given any sequence $\{N_1, N_2, N_3, \ldots\}$ of positive integers, there is a solution with N_1 spikes in the first burst interval, N_2 spikes in the second burst interval, N_3 spikes in the third burst interval, and so on. Moreover, the solutions are ordered lexicographically by the wave speed ω in the following sense. Suppose that $\{N_1, N_2, N_3, \ldots N_K \ldots\}$ and $\{M_1, M_2, M_3, \ldots M_K \ldots\}$ represent two such solutions, with speed ω_N and ω_M, respectively. If we compare these sequences term-by-term, N_1 with M_1, N_2 with M_2, and so on, there always is a first pair of terms that differ unless the sequences are identical. Denote this first pair by (N_K, M_K). Then $\omega_N < \omega_M$ if and only if $N_K < M_K$. More complex, even chaotic, waveforms are also possible, again under special hypotheses but without adding any more variables to the model.

I.10. Parabolic and Paroxysmal Bursts: Augmented Hodgkin-Huxley Models

There exist bursting patterns *in vivo* that are not consequences of the basic Hodgkin-Huxley dynamics with three ionic variables m, n, and h. Some of these bursts can, however, be generated by Hodgkin-Huxley models with four ionic variables. Figure 11A depicts a periodic bursting pattern of this type, the so-called *parabolic* bursts that

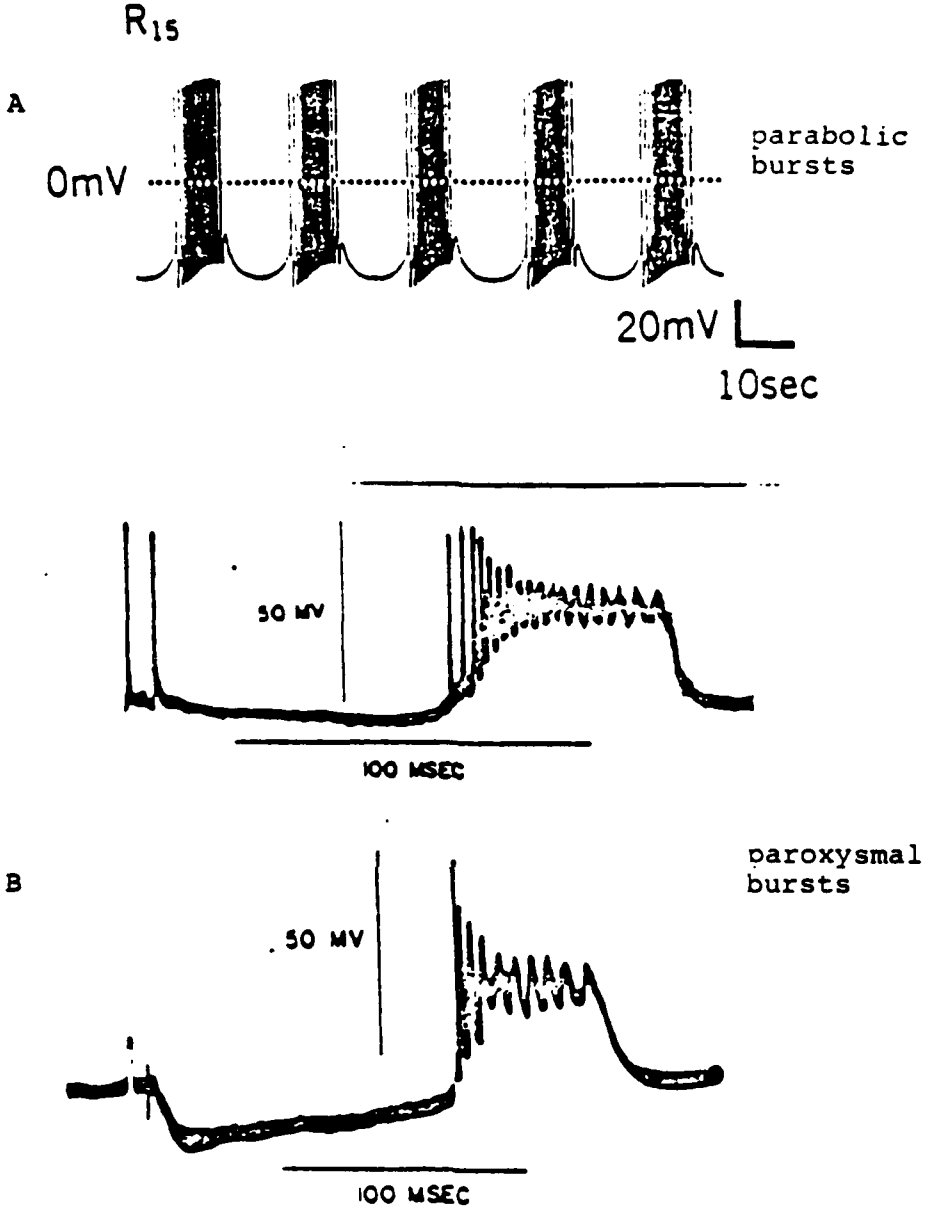

Figure 11: (A) Parabolic bursts in Aplysia abdominal ganglion (Roberge, et al, 1978, p.392).
(B) Paroxysmal bursts in the cat hippocampus (Kandel and Spencer, 1961, p.245).

have been studied in the Aplysia abdominal ganglion (Roberge, et al, 1978, p.392). Within a parabolic burst, the spiking frequency first increases, then decreases, before shutting off. The first part of the parabolic burst, wherein spiking frequency increases, resembles an HH burst (Figures 8A and 8C). Due to this fact, a parabolic burst form

can be generated if there exists another slow process acting on the time scale of seconds, rather than the millisecond time scale of the Hodgkin-Huxley currents, that interacts with the three faster currents. Because the time scale of this additional process is relatively slow, it acts like a parametric change that moves the burst away from its Ω-periodic solution towards the rest point and thereby slows the frequency of spikes before the burst terminates (Carpenter, 1979). Either a slow accumulation of extracellular potassium or an additional slow potassium current can produce this effect (Faber and Klee, 1972).

Paroxysmal bursts, depicted in Figure 11B, occur in cell bodies rather than being propagated down axons (Kandel and Spencer, 1961). Such a burst pattern can formally be generated by antidromic (backwards) flow of potential from the cell body to the cell dendrites which, in turn, further depolarize the cell body and raise the baseline of burst activity to its plateau level.

A related type of burst which rides a plateau is illustrated in Figure 12. This periodic bursting solution is generated by periodic

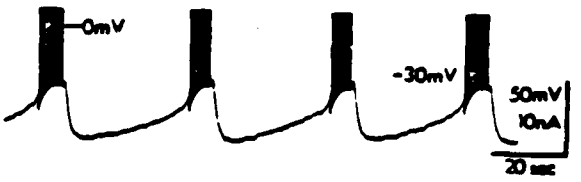

Figure 12: A burst riding the crest of a slow potential wave (Otala lactea, cell 11) (Barker and Smith, 1978, p.380). The large oscillations in the baseline potential are not part of HH bursts, although small oscillations may be present.

pacemaker activity, or a slow depolarization shift, (DPS), on which spikes are superimposed when the potential is suprathreshold. Here the

mechanisms of interest are those which generate the DPS, rather than the spikes per se. This is the type of burst discussed in Plant and Kim (1975).

I.11. FitzHugh-Nagumo Bursts

Burst solutions have recently been reported to occur in the FitzHugh-Nagumo model (Evans, Fenichel, and Feroe, 1982; Feroe, 1982; Hastings, 1982). This model is similar to a generalized Hodgkin-Huxley model with two rather than three ionic processes. It was originally motivated by the observation that since potassium activation (n) tends to increase while sodium inactivation (h) tends to decrease, the sum n+h does not vary too much (FitzHugh, 1961; Nagumo, Arimoto, and Yoshizawa, 1962). Hence one degree of freedom was removed from the original Hodgkin-Huxley model by assuming that n+h is identically constant. Other simplifications in the model were made to represent it as a tunnel diode.

In vivo, the processes of sodium inactivation (h) and potassium activation (n) are relatively slow. In the Hodgkin-Huxley model, this fact becomes the mathematical hypothesis that the model's eigenvalues are real numbers. A necessary requirement for the Evans et al (1982) and Hastings (1982) analysis is that the corresponding process in the FN model be fast in order to create eigenvalues that are complex numbers. In the original HH model, n and h could only change this quickly if the model's temperature variable were set at twice the normal temperature (Centigrade).

Independent of discussions about the physical plausibility of the FN-burst hypothesis, one can test for FN bursts and HH bursts in vivo by their parametric properties. FN bursts are obtained by perturbing off a single spike, so the spikes within such a burst are evenly and widely spaced, by contrast with the typical speed-up of HH bursts de-

picted in Figures 8A and 8C.

II. THE TRANSDUCTION OF LIGHT BY VERTEBRATE PHOTORECEPTORS

II.1. The Turtle Cone and the Dynamics of Chemical Transmitter Substances

In this section we consider the electrical response of cells in another model system, the turtle cone. The discussion will have several points in common with the previous section on single nerve cell dynamics. The turtle cone, like the squid axon, is important not just in itself, but because it is a convenient experimental preparation in which to investigate a general neural phenomenon: the transduction of light into an electrical response. Many experiments have indicated that this transduction process is mediated by a chemical transmitter within the photoreceptor. Our discussion will compare two models for the interactions of light, transmitter, and photoreceptor potential: the unblocking model of Baylor, Hodgkin, and Lamb (BHL) (1974b) and our own gating model (Carpenter and Grossberg, 1981).

As with the Hodgkin and Huxley work on the squid giant axon, the generative work on turtle cones includes an exhaustive series of parametric experiments (Baylor and Hodgkin, 1973, 1974; Baylor, Hodgkin, and Lamb, 1974a, 1974b) that led to the unblocking model. Both the unblocking model and the Hodgkin-Huxley model begin with the basic membrane equation, which is then augmented by auxiliary equations. Our

analysis of turtle cone dynamics will, however, be very different from the analysis in Section I. In their article, Baylor, Hodgkin, and Lamb (1974b) do an extensive numerical analysis of their model, and note that, despite its complexity, it fails to meet important data. Their model's difficulties seem to center on how the chemical transmitter mediates between light and potential. We realized that an alternative model of transmitter dynamics (Grossberg, 1968, 1969) could provide intuitively simpler and better quantitative fits to the turtle cone data. This gating model has additional appeal to us because it was derived from a general principle of neural design and has been helpful in explaining transmitter-mediated data in a variety of other neural systems (Grossberg, 1975, 1980, 1982a,b).

Thus in this section, our discussion will approach the problem of how to choose between two models of a complex biological phenomenon. This task is rendered all the more difficult by the fact that the light transduction process involves multiple stages that are difficult to experimentally disentangle. No model can hope to include all the interactions that will eventually be disclosed by ever finer physiological, biochemical, and molecular techniques.

We approach this task by offering parametric predictions that can characterize whether the type of transmitter gating process that we have in mind is rate-limiting in any body of data, whether in a photoreceptor or not. Thus our approach is to explicate the parametric implications of a basic neural design no less than to try to understand a particular body of data. In the case of vertebrate photoreceptors, experimental articles based on electrophysiological recording typically interpreted the major electrical effects to occur in the outer segment of the photoreceptor. More recent experiments using suction electrodes that can electrically isolate the photoreceptor outer segment from its inner segment suggest that these electrical effects are not

necessarily localized at the outer segment (Nunn, Matthews, and Baylor, 1980; Yau, McNaughton, and Hodgkin, 1981). Our analysis does not attempt to specify the anatomical locations at which a transmitter or transmitters may act, but rather provides parametric evidence for whether a rate-limiting transmitter gating step occurs at some stage in the generation of photoreceptor potential.

II.2. The Unblocking Model

Figure 13 illustrates a schematic version of the first stages of vertebrate photoreceptor dynamics, as represented by BHL. Light enters

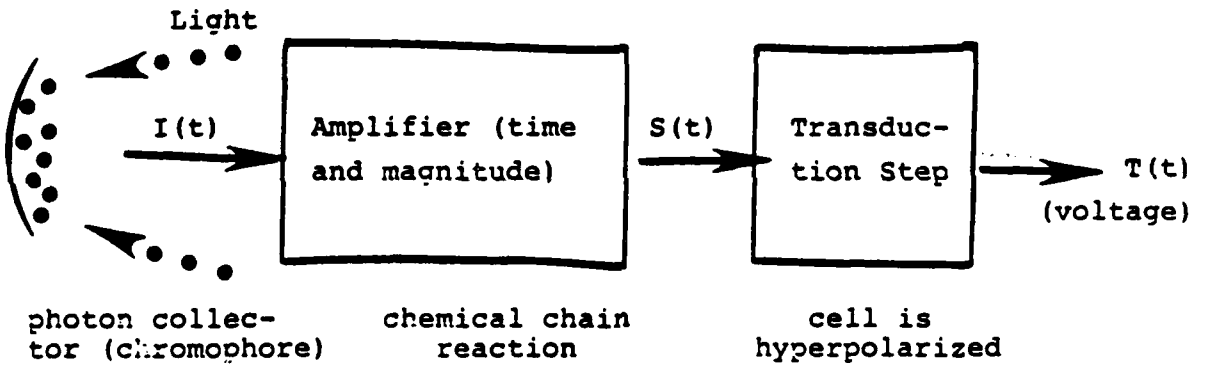

Figure 13: Schematic view of the early stages of light processing in the vertebrate photoreceptor.

the front of the eye, and photons are collected at the back of the eye, in the chromophore. The light signal, I(t), is amplified, both in time and magnitude, by a chemical chain reaction. Such an amplification step

enables the eye to register even 1 or 2 photons by generating enough activity to translate these microscopic signals into a voltage change which can be transmitted to the brain. The output of the chain reaction is S(t). Next comes the transduction transformation

$$S(t) \rightarrow T(t) \tag{14}$$

whereby the photoreceptor is hyperpolarized by light and the electrical signal T(t) is generated. The signal T(t) influences the activity of subsequent retinal layers and the brain. We will focus our attention on the transduction transformation (14).

The BHL model of the transduction transformation is summarized below.

Membrane Equation:

$$\tau_L \frac{dV}{dt} = E - V(1 + G_f + G_i) \tag{15}$$

Light-Sensitive Ionic Conductance:

$$G_i = \frac{\bar{G}_i}{1 + \frac{z_1}{K}} \tag{16}$$

Time-Average of Prior Voltage Transform:

$$\tau_f \frac{dG_f}{dt} = F(V) - G_f \tag{17}$$

Logistic Transform of Voltage:

$$F(V) = \frac{\bar{G}_f}{1 + \exp\left[\frac{(V-V_f)}{V_s}\right]} \tag{18}$$

Linear Chain Reaction to Light:

$$\left(\frac{d}{dt} + \alpha\right)^{n-1} y_{n-1} = \alpha^{n-2} I(t) \tag{19}$$

Blocking Substance:

$$\frac{dz_1}{dt} = \alpha y_{n-1} - \kappa_{12} z_1 + \kappa_{21} z_2 \tag{20}$$

Unblocking Substances:

$$\frac{dz_2}{dt} = \kappa_{12} z_1 - (\kappa_{21}+\kappa_{23}) z_2 + \kappa_{32} z_3 \tag{21}$$

$$\frac{dz_3}{dt} = \kappa_{23} z_2 - (\kappa_{32}+\kappa_{34}) z_3 \tag{22}$$

Gain Control:

$$A\kappa_{21} = \kappa_{12} = \bar{\kappa}_{12} + \nu z_2 \left[\frac{\kappa_{12M} - \bar{\kappa}_{12}}{\kappa_{12M} - \bar{\kappa}_{12} + \nu z_2}\right] . \tag{23}$$

Just as in the HH model, V(t) in (15) is the transmembrane voltage. In the BHL model, however, V(t) is assumed to be spatially homogeneous; possible spatial interactions of different photoreceptor segments are not considered. Function G_i in (15) and (16) is a light-sensitive ionic conductance. In (16), G_i is a decreasing function of z_1 which represents the concentration of a blocking substance that is hypothesized in (20) to be the output of the light-initiated chain reaction

$$I(t) \rightarrow y_1 \rightarrow y_2 \rightarrow y_3 \rightarrow \cdots \rightarrow y_{n-1} \rightarrow z_1 \tag{24}$$

that is defined by (19). According to equations (15), (16), (19) and (20), light increases the amount of blocking substance and thereupon

hyperpolarizes the membrane by decreasing G_i in (15).

The blocking substance z_1 is removed by the unblocking substances z_2 and z_3 according to equations (20)-(23). At first glance, the blocking-unblocking equations (20)-(22) appear to be linear. However the z_2 terms in the definitions of κ_{12} and κ_{21} in (23) show that equations (20)-(22) are highly nonlinear. The blocking-unblocking hypothesis is the key component of the BHL model.

The conductance G_f in (15) also depends nonlinearly on the voltage V via equations (17) and (18). Its significance in the BHL model will be reviewed when we discuss relevant data in Section II.5.

II.3. The Gating Model: Unbiased Transmitter-Mediated Signalling

The gating model of the transduction transformation can be derived as an answer to the following question:

What is the simplest law whereby one nerve cell site can send unbiased signals to another nerve cell site?

If S(t) is the input to one cell site and T(t) is the output to the next cell site, then a linear relationship such as

$$T = SB \tag{25}$$

is clearly the simplest law for unbiased transmission, where B is a positive constant. Here the outgoing signal T is directly proportional to the incoming signal S, so the signal is relayed perfectly.

This is not the end of the discussion when the output signal T(t) is due to the release of a chemical transmitter substance z(t) in response to the input signal S(t). Then we must face the issue of how a large and sustained signal S(t) is prevented from depleting z(t) and thereby causing a progressively smaller signal T(t).

From this perspective, equation (25) may be replaced by the pair

of equations

$$T = Sz \tag{26}$$

and

$$z = B. \tag{27}$$

Equation (26) says that transmitter z is released at a rate (proportional to) T in response to signal S. In other words, z gates S to generate T, or T is caused by a mass action interaction between S and z. By (26), more transmitter is released if either the incoming signal S or the amount of available transmitter z is increased.

Equation (27) simply requires that the amount of transmitter seek a constant level B, as in (25), so that the sensitivity of T to S will not decrease due to transmitter loss. If equations (26) and (27) can be simultaneously implemented, then the perfect transmission described by equation (25) will be assured. The gating model is derived from hypotheses that aim to maintain unbiased transmission when the cell sites in question signal each other via a depletable chemical transmitter. Herein lies the intuitive appeal and generality of the gating concept.

The simplest dynamical equation that is capable of simultaneously summarizing equation (26) and (27) is the following:

Transmitter Accumulation-Depletion Equation

$$\frac{dz}{dt} = A(B-z) - Sz \ , \tag{28}$$

where A,B 0. In (28), term A(B-z) says that z accumulates until it reaches the target level B, as required by (27). Term -Sz says that transmitter is depleted at the rate T, as required by (26).

II.4. Unbiased Transmission by Miniaturized Cells: Light-Induced Enzymatic Activation of Transmitter Accumulation

Equation (28) is the simplest dynamical law that might possibly subserve unbiased chemical transmission between cell sites, but it is not adequate in cells that possess certain properties shared by photoreceptors. This is because the rate of transmitter accumulation (A) in term A(B-z) may be small compared to the rate of transmitter depletion (S) in term -Sz if the signal S can become large, as in a photoreceptor that can respond to a wide dynamical range of light intensities I(t). Then z(t) can become depleted significantly below its asymptotic level B, and loss of sensitivity in T's response to S can occur. Thus equation (28) alone does not solve the following.

Problem: A large input signal S(t) can deplete z(t) and cause habituation or desensitization of T(t).

How can a cell maintain its sensitivity in spite of large fluctuations in light input intensity? Two types of solution can be contemplated in (28). The first solution, which we do not adopt, leads to the type of reaction to light that is schematized by the BHL chain reaction (24) leading from light input I to transmitter reaction z_1.

If a large storage depot of transmitter is maintained, then even large signals S will deplete only a small fraction of the depot. Hence, if $B >> 1$, then even large (but bounded) signals S will cause only a small reduction in the ratio zB^{-1}.

If a large storage depot of transmitter existed within each photoreceptor, then this depot would enlarge each photoreceptor's volume, and would thereby reduce the number of photoreceptors that could be packed into a fixed retinal area. Improving the dynamical sensitivity of each photoreceptor using this method would reduce the spatial sensitivity of the retina as a whole.

We can therefore reformulate our design problem as follows.

Problem: How can a spatially miniaturized photoreceptor maintain its sensitivity to large fluctuations in input intensity?

If in equation (28), B is not large relative to S, then an alternative solution is to let the rate of transmitter accumulation (A) increase as a function of S to counterbalance the rate S of transmitter depletion. Otherwise expressed, we suppose that there exists a light-induced enzymatic activation of the transmitter accumulation rate. According to this hypothesis, the effects of light on the photoreceptor do not merely follow a serial chain of transduction steps. Rather, light activates parallel pathways which later mutually interact to generate the cone potential.

The simplest mass action law for a light-activated accumulation rate is

$$\frac{dA}{dt} = -C(A-A_o) + D[E-(A-A_o)]S. \qquad (29)$$

Here, A_o is the baseline level of A(t) in the dark (S=0). An incoming light-induced signal S tends to drive the accumulation rate A(t) towards its maximal level A_o+E.

We have found that the two equations (28) and (29) numerically fit the most difficult BHL data better than the full BHL model (15)-(23). Indeed a single equation derived from (28) and (29) fits these data better than the full BHL model. This is true even if these equations are coupled to the cone potential V(t) in the simplest possible way by making the change in T proportional to the change in V. Wherever such a coupling or more realistic couplings occur, whether in the outer segment or the inner segment, does not influence the meaning of the gating step or the goodness of numerical fit.

The simpler gating model assumes that enzymatic activation occurs quickly relative to z's equilibration rate. Then A in (29) is always

approximately at its equilibrium level

$$A(S) = A_o + \frac{EGS}{1+GS} \tag{30}$$

where $G \equiv DC^{-1}$. This approximation leads to

Gating Model I

$$T = Sz \tag{26}$$

$$\frac{dz}{dt} = A(S)(B-z)-Sz \tag{31}$$

where A(S) is defined by (30). When the enzymatic activation of A proceeds at a finite rate relative to z's equilibration rate, we study the

Gating Model II

$$T = Sz \tag{26}$$

$$\frac{dz}{dt} = A(B-z)-Sz \tag{28}$$

and

$$\frac{dA}{dt} = C(1+GS)[A(S)-A], \tag{29}$$

where A(S) is defined by (30).

II.5. Double Flash Experiments

An important difference between the chain reaction of the BHL model

$$I - y_1 - y_2 - \ldots - y_{n-1} - z_1 - \tag{24}$$

and a chain reaction of a gating model

$$I \rightarrow y_1 \rightarrow y_2 \rightarrow \ldots \rightarrow y_{n-1} = S \rightarrow Sz \rightarrow \qquad (32)$$

is illustrated by a double flash experiment (Figure 14). Baylor, Hodgkin, and Lamb (1974a) found that a bright flash causes the potential

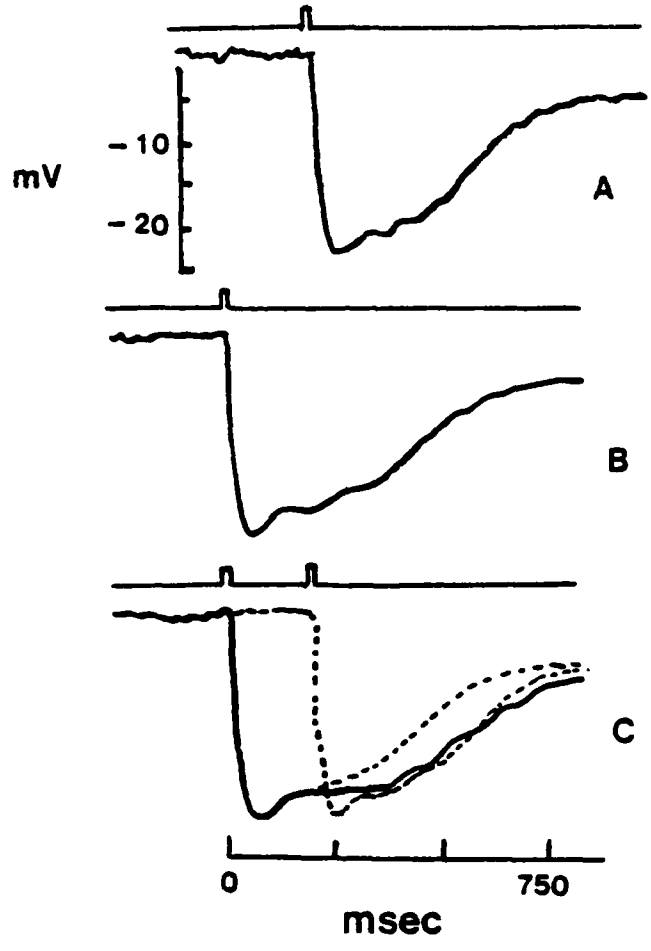

Figure 14: Effect of a bright conditioning flash on the response to a subsequent bright test flash. (A) Response to test flash alone. (B) Response to conditioning flash alone. (C) Response to both flashes, with the upper two responses dotted in. Redrawn from Figure 15 (Baylor, Hodgkin, and Lamb, 1974a, p.716).

to overshoot before settling to a plateau level that is maintained for a while before the potential returns to equilibrium. A second bright flash that occurs while the potential is at the plateau value caused by the first flash does not cause an overshoot even though it does extend the duration of the chain reaction.

Given a chain reaction like (24), it is not possible to understand how the duration of the chain reaction can be prolonged without increasing the concentration of internal transmitter (Detwiler, Hodgkin, and McNaughton, 1980, pp.222-223). Since, however, the voltage does not change in response to this change in transmitter concentration, the voltage must be saturated, or insensitive to, the transmitter increment. In the BHL model, the definition of the conductance G_f in equations (15), (17), and (18) is made to guarantee the voltage's insensitivity to a second flash.

Notwithstanding the possible physical truth of these assertions, the gating model provides an alternative explanation: The transmitter term z in the chain reaction (32) can equilibrate via equation (28) or (31) to the first flash, thereby causing an overshoot in potential, and can thereafter remain insensitive to a second flash that occurs while S remains at its plateau value, without preventing the new flash from prolonging the duration of the chain reaction. See Carpenter and Grossberg (1981, pp.15-16) for further details. This is perhaps the critical difference between an unblocking model and a gating model. A more critical test between the models might be made using a parametric series of double flash experiments in which the second flash is twice as intense as the first.

The remainder of this review of photoreceptor models will compare how the unblocking and gating models fit a demanding body of parametric data, how the gating step can be coupled to a membrane equation, and how the gating model can be parametrically tested by blocking the

light-induced enzymatic activation step.

II.6. Parametric Studies of Flashes on Backgrounds: Differential Reactions in the Energy and Time Domains

A critical series of parametric experiments which generated paradoxical data was reported in Baylor and Hodgkin (1974). The Gating Model I with just one dynamical equation fits these data better than the full BHL model. The Gating Model II with two dynamical equations provides a significantly better fit. In these experiments, (Figure 15), a brief (11 msec.) flash of fixed size (δ) is superimposed on a constant level of background illumination (I_o). The cone potential is

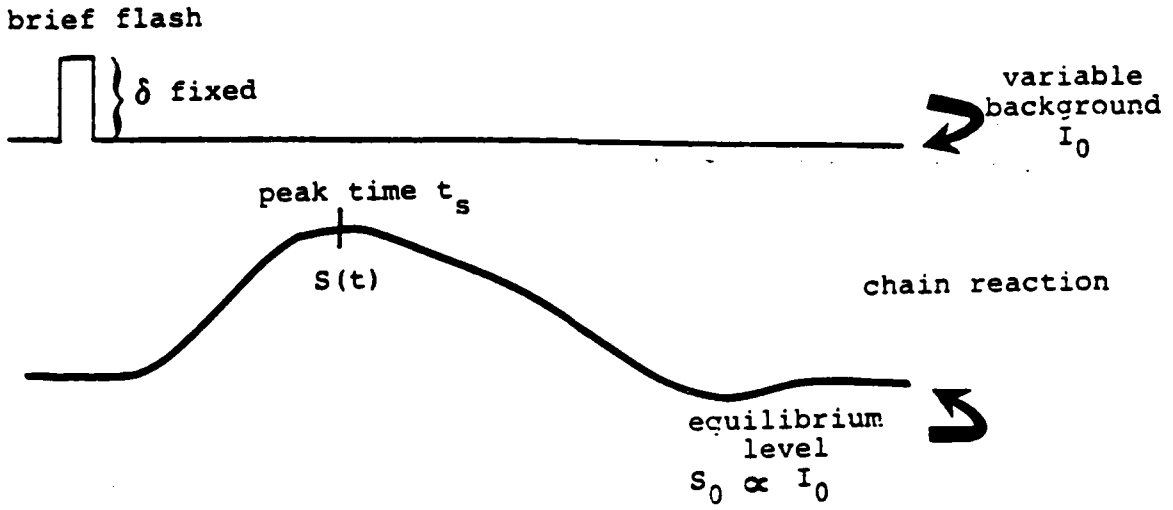

Figure 15: This experiment, from (Baylor and Hodgkin, 1974), measures the photoreceptor's response to a brief flash of fixed size, superimposed on a level of background light which ranges from dark to very bright.

allowed to equilibrate to the background level I_o before the flash occurs at time t=0. As I_o is parametrically increased across several

log units, the cone's voltage responses to the fixed flash are measured for $t \geq 0$. The results of these experiments are plotted in Figure 16a. Each curve in Figure 16a represents the amount of hyperpolarization caused by the flash relative to the baseline level of hyperpolarization caused by the background level I_o.

As I_o is increased, the peak hyperpolarization decreases, as is intuitively plausible. However, the <u>times</u> at which these peak responses occur first decrease as I_o increases, but then, at sufficiently large values of I_o, begin to increase. Thus a monotonic change in the energy domain coexists with a non-monotonic change in the time domain. Such a differential parsing of energy and time also occurs in the double flash experiments (Section II.5) wherein a second flash influences temporal but not energetic measures, by contrast with a first flash.

Numerical solutions of the BHL model are shown in Figure 16b. Note that the scales in the lower two graphs differ from those in Figure 16a, and that the peak sizes are off by a factor of 10 in the lowest graph. Also the turnaround occurs at too low a light intensity, and the time of the turnaround is too late.

Results for the Gating Model I are given in Figure 16c. Here, the peak sizes at large I_o are also off by a factor of 10, but the time and intensity of the turnaround are closer to the data. Recall that Model I consists of a single linear differential equation.

Results for the Gating Model II, in Figure 16d, fit the data well: peak size, turnaround time, and light intensity at the turnaround are all close to those in Figure 16a. The times at which peak response occurs, as functions of log I_o, are plotted in Figure 17 for the Baylor-Hodgkin (1974) data, the BHL model, and the two gating models.

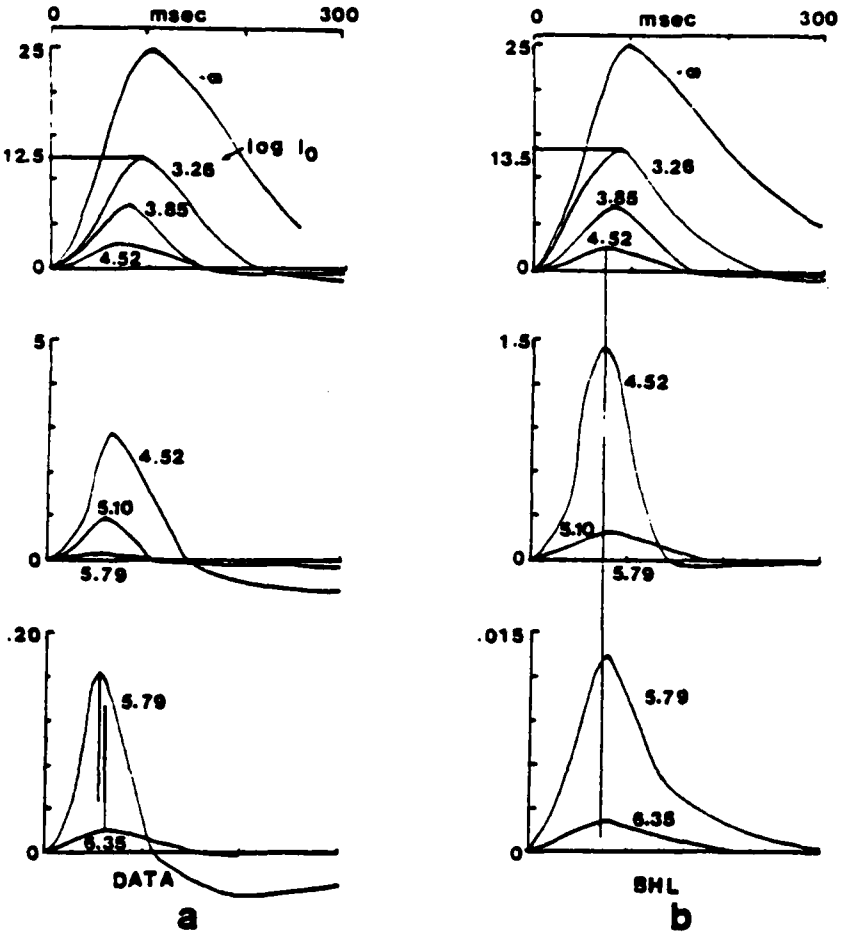

Figure 16: Intracellular response curves $x(t)-x_o$ showing the effect of a flash superimposed on a background light of fixed intensity, I_o. Each horizontal axis represents the time, in msec., since the middle of the 11 msec. flash. Each vertical axis is scaled so that the peak value of $x(t)-x_o=x(t)$ in the dark is equal to 25. The number beside each curve equals $\log_{10}(I_o)$, where I is calibrated so that when $\log_{10}I_o = 3.26$, the peak of $x(t)-x_o$ equals 12.5. (a) The Baylor-Hodgkin (1974) data. (b)The Baylor-Hodgkin-Lamb model predictions redrawn from (Baylor, Hodgkin, and Lamb, 1974b, p.785).

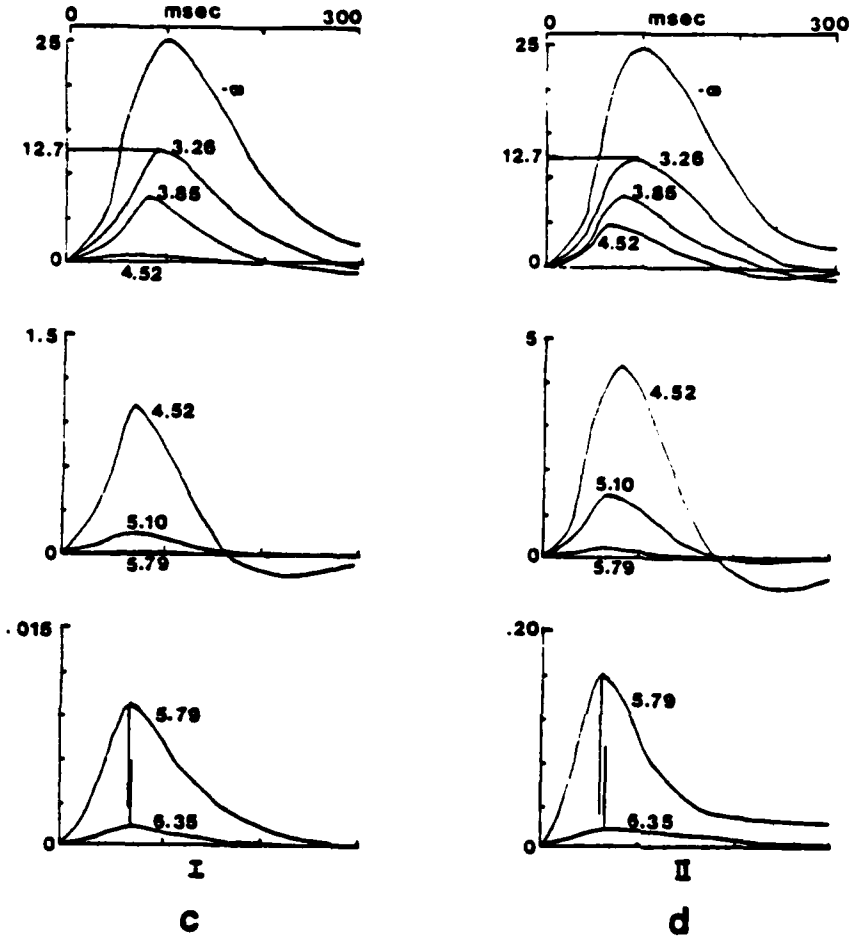

Figure 16 (cont.): (c) Predicted response of Gating Model I (Equation (9)). (d) Predicted response of Gating Model II (Equations (7)-(8)). For each of Models I and II, $x(t)$ is proportional to $S(t)z(t)$. Note that the vertical scales of (a) and (d) are the same, and the vertical scales of (b) and (c) are the same.

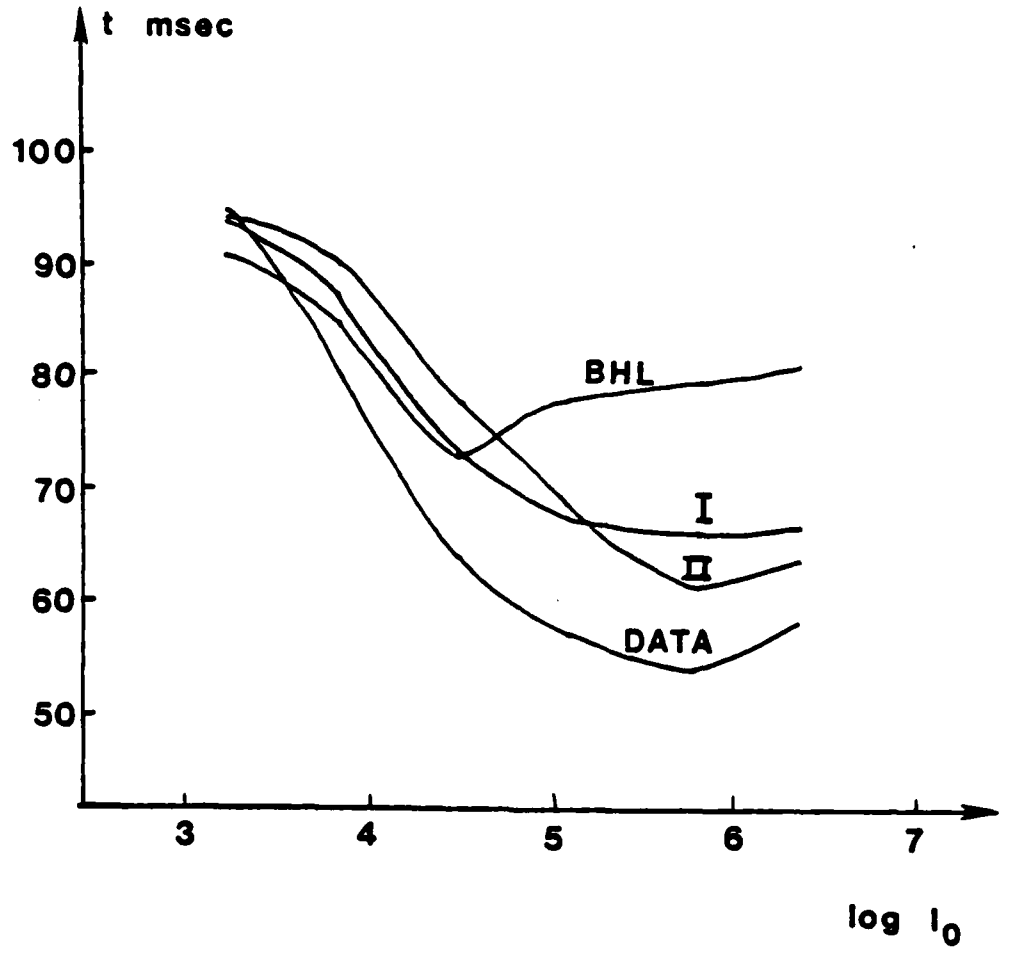

Figure 17: Times at which the peak hyperpolarizations occur for the Baylor-Hodgkin (1974) data and the three models. Note that the input intensity at which the turnaround occurs and the dynamic range of peak times are much too small in the BHL model. Baylor, Hodgkin, and Lamb (1974b) considered this the most serious defect of their model.

II.7. Locus of the Transmitter Gating Stage

The model thus far has described only chain reaction and transmitter gating effects in keeping with our hypothesis that the gate is the rate-limiting cause of phenomena like the turnaround of potential peaks. Both conceptual completeness and the explanation of various other phenomena require that the gating step be coupled to the cone potential. For example, Baylor, Hodgkin, and Lamb (1974a) found during double flash experiments that an extra slow conductance accompanies the overshoot to the first flash but not the prolonged response, without overshoot, to the second flash. In the unblocking model, this property requires the hypothesis that an extra membrane channel exists

with properties that control the slow conductance term. In a gating model, a slow conductance effect is found without hypothesizing an extra membrane channel (Carpenter and Grossberg, 1981, p.22). The slow conductance and its relationship to the overshoot of potential follow directly from the coupling of the gate to the potential.

Such properties of the gating model are invariant under model variations which place the coupling between gate and potential at different stages in the light transduction process. This fact is important to realize because electrophysiological data leave uncertain the exact stage at which a particular biochemical process occurs. This uncertainty has recently been reduced by the use of suction electrode methods that permit outer segment recordings to be made in isolation from inner segment electrical signals (Baylor, Lamb, and Yau, 1979). These methods suggest that various processes which produce overshoot phenomena occur in the inner segment, rather than the outer segment, as had previously been thought (Baylor, Lamb, and Yau, 1979; Nunn, Matthews, and Baylor, 1980). This modification in the locus of overshoot-related phenomena is compatible with the existence of a rate-limiting gating step, but indicates that such a step occurs later in the transduction process than previous data suggested.

II.8. Coupling the Transmitter Gate to Cell Potential

A gating signal can, in principle, either depolarize or hyperpolarize a cell's potential. Although this distinction is of great physical importance, many formal properties are the same in both cases. For example, S(t) can be thought of either as the output of the chain reaction or as the effect of the chain reaction on the outer segment potential. Whichever interpretation of S(t) is used, the gated signal T(t) may then, in principle, either depolarize or hyperpolarize the cone potential. Whatever interpretation is needed to treat a particu-

lar case, the steady-state amount of hyperpolarization or of depolarization in response to a gated signal T=Sz is of the form

$$\frac{MT}{N+T} \cdot \tag{33}$$

The rate with which the potential approaches asymptote (33) will depend on whether the cell is hyperpolarizing or depolarizing. However, in cases where the potential reacts quickly relative to the gate's reaction rate, as we assert occurs in turtle cones, the potential change maintains the approximate equilibrium (33) whether the cell is hyperpolarized or depolarized. In this case, the time and the background intensity at which the potential, via (33), experiences a turnaround in potential peak is approximately the same as the time and the background intensity at which the gated signal T itself experiences its turnaround. In fact, (33) is approximately proportional to T except if it begins to saturate at values of T >> N.

The gating model is coupled to the membrane equation as follows. We start with the spatially uniform version of the membrane equation for the voltage V(t):

$$C_0 \frac{dV}{dt} = (V^+ - V)g^+ + (V^- - V)g^- + (V^p - V)g^p \ , \tag{34}$$

where V^+, V^-, and V^p are the excitatory, inhibitory, and passive saturation points; and g^+, g^-, and g^p are the corresponding conductances.

To couple the excitatory conductance g^+ to the gated signal T=Sz, we use a simple mass action law. Below we describe the case wherein an increase in T decreases g^+, and thereby hyperpolarizes V. Similar qualitative results are obtained if T increases rather than decreases g^+. One difference between the two couplings is that a hyperpolarizing coupling decreases V's reaction rate, whereas a depolarizing coupling

increases V's reaction rate.

The simplest mass action hyperpolarizing action is defined by

$$\frac{dg^+}{dt} = H(g_0 - g^+) - Jg^+T \ , \tag{35}$$

where g_0 is the maximal number of open pores in the dark (T=0). Equation (35) says that closed pores, which number g_0-g^+, open at a rate H; and that the gated signal T closes open pores, which number g^+, at a rate J. Equation (35) can be rewritten in the form

$$\frac{dg^+}{dt} = H(1 + KT)\left[\frac{g_0}{1+KT} - g^+\right] \tag{36}$$

where $K = JH^{-1}$. If pores g^+ close quickly relative to the reaction rate of the gate z to light, then (36) implies that

$$g^+(t) \equiv \frac{g_0}{1+KT} \ . \tag{37}$$

Assuming that pores close quickly, as in (37); that $g^-(t)$ is constant, say $g^-(t) \equiv g_1$; and setting $C_0 = 1$ and $g^P = 0$ for simplicity, the membrane equation (34) becomes

$$\frac{dV}{dt} = (V^+ - V)\frac{g_o}{1+KT} - (V - V^-)g_1 \ . \tag{38}$$

The equilibrium potential V_0 can be found by setting T=0 and $\frac{dV}{dt} = 0$ in (38). It is

$$V_0 = \frac{V^+g_0 + V^-g_1}{g_0 + g_1} \ . \tag{39}$$

The amount of hyperpolarization

$$x = V_0 - V \tag{40}$$

then obeys the equation

$$\frac{dx}{dt} = -\left(g_1 + \frac{g_0}{1+KT}\right)x + \frac{LT}{1+KT} , \tag{41}$$

where

$$L = Kg_1(V_0 - \bar{V}) . \tag{42}$$

Equation (41) can, in turn, be written in the form

$$\frac{dx}{dt} = \left(g_1 + \frac{g_0}{1+KT}\right)\left(\frac{MT}{N+T} - x\right) , \tag{43}$$

where

$$M = V_0 - \bar{V} \tag{44}$$

and

$$N = \frac{g_0 + g_1}{g_1 K} . \tag{45}$$

If x(t) reacts quickly relative to the reaction rate of z(t), then (43) implies

$$x(t) \approx \frac{MT(t)}{N+T(t)} , \tag{46}$$

as in (33).

When equation (46) is written in the form

$$\frac{Nx}{M-x} = T , \tag{47}$$

it provides a basis for comparison with the Baylor, Hodgkin, Lamb (1974b) equation

$$\frac{aU}{U_L - U} = \frac{z_1}{K} \tag{48}$$

relating amount of hyperpolarization U (in their notation) to the blocking variable z_1. In the gating model, the gated signal T = Sz replaces z_1.

II.9. Tests of Enzymatic Activation

Another point of comparison between the gating model and the unblocking model arises by considering the steady-state reactions of both models to a series of background lights. In the gating model, equations (26), (28), (29), and (30) imply a dependence of the form

$$T = \frac{PS(1+QS)}{1+RS+US^2} \tag{49}$$

where coefficient U is small compared to QR (Carpenter and Grossberg, 1981, p.12, p.21). In the unblocking model, the dependence is of the form

$$\frac{z_1}{K} = \frac{PS(1+QS)}{1+RS} \; . \tag{50}$$

Again the gated signal T in (49) replaces the blocking variable z_1 in (50). Equation (49) also contains the quadratic term US^2. No such term appears in the unblocking equation (50), which shows that this equation must break down at large values of S, since the amount of blocking substance must be bounded, whereas the right-hand side of (50) grows without bound as S increases.

In the gating model, the quadratic terms QS and US^2 are due to

the light-induced enzymatic reaction (29). If the enzymatic activation could be chemically inhibited, then the steady-state gating equation (49) would reduce to the equation

$$T = \frac{PS}{1+RS} , \tag{51}$$

wherein no quadratic terms occur. Simultaneously, the turnaround of potential peaks due to light flashes on parametric increases of background light would cease to occur; only a monotonic decrease in the time to peak should be observed. Finally, suppose that the steady-state potential is plotted against the logarithm of light intensity after adapting the cone to a series of prior background intensities. Then the cone's potential at a given log intensity is shifted as a function of background intensity. Inhibition of the enzymatic step should reduce the size of the shift due to high intensity lights by a predictable amount (Carpenter and Grossberg, 1981, pp.24-25). These and related parametric predictions can be used to test for the existence of a rate-limiting enzymatically modulated transmitter gating step in photoreceptor and related cellular preparations.

III. CIRCADIAN RHYTHMS AND OTHER BIOLOGICAL CLOCKS

III.1. A Chemical Gating Model of Circadian Rhythms and Motivational Cycles

Because the gating concept can be derived from general principles about unbiased chemical transmission between cells (Section II.3), it should not be surprising that chemical gates may be found in a wide variety of neural systems. Whenever such a general principle can be identified, a classification of the properties whereby the principle manifests itself in data is desirable. Our discussion of photoreceptor dynamics has reviewed a type of data which exhibits parametric properties akin to those of an enzymatically activated rate-limiting transmitter gating step in a feedforward chain reaction. In such a reaction chain, one does not expect to find spontaneous large amplitude oscillations or sustained oscillations in response to brief inputs. When chemical gates are placed in feedback anatomies, by contrast, a wide variety of oscillations can occur.

A role for gates in feedback anatomies first arose in models of motivated behavior (Grossberg, 1972a, 1972b, 1975, 1980, 1982a, 1982b, 1982c). The model of circadian rhythms that we introduce here for the first time shares many formal similarities with these earlier models of gated feedback networks. These similarities clarify a sense in which motivated behaviors are controlled by a hierarchy of similar mechanisms with a circadian pacemaker at the foundation of the hierarchy, and permit us to understand how rhythmic properties arise in the motivated behaviors themselves (Moore-Ede, Sulzman, and Fuller, 1982, p.186). Due to the role of slow chemical gates in generating these rhythms, our model allows us to understand why certain chemical transmitters can oscillate according to a circadian rhythm, not only because they are driven by pacemaker output, but also because they

form an integral part of the rhythm-generating mechanism (Binkley, 1979; Deguchi, 1979; Jouvet, 1974; Lewy, Wehr, Goodwin, Newsome, and Markey, 1980; Markowitz, Rotkin, and Rosen, 1981; Nestler, Zatz, and Greengard, 1982; Passouant and Oswald, 1979; Takahashi, Hamm, and Menaker, 1980; Tapp and Holloway, 1981; Wehr and Wirz-Justice, 1982; Zatz and Brownstein, 1979).

Three different biological processes, properly juxtaposed, are necessary to define a gated pacemaker: slow chemical gates, feedback, and competition. If any one of these processes is removed, a gated pacemaker ceases to oscillate. Using these ingredients, we have defined a pharmacologically predictive model of a circadian pacemaker. In their 1978 article, Daan and Berde note the essential weakness of previous models: "Most models of circadian oscillators have been abstract, in the sense that they include parameters not definable in terms of concrete physiological or biochemical processes...This feature makes them difficult to test and limits their heuristic or predictive value"(p.299). Because our model is physiologically grounded, it enables us to provide a unified explanation of circadian properties that have not previously been dynamically explained, such as period doubling, bimodal activity patterns, rhythm splitting, long-term after-effects, Aschoff's rule and its exceptions, characteristic phase leads and lags, seasonal modulation of activity, and differences between nocturnal and diurnal animals (Aschoff, 1960, 1979; Enright, 1980; Jouvet, Mouret, Chouvet, and Siffre, 1974; Moore-Ede, Sulzman, and Fuller, 1982; Pittendrigh, 1960, 1974; Wever, 1979; Winfree, 1980). For example,concerning long-term after-effects, Pittendrigh (1974) wrote in an important review article: "They are more widespread than the current literature suggests; they are not accounted for by any of the several mathematical models so far published; and they must be reckoned with in the mechanism of entrainment"(p.441). Our work

pays particular attention to after-effects and provides examples of all the after-effect phenomena that Pittendrigh (1974) discusses.

III.2. Some Alternative Circadian Models

As with the classification of signal patterns in terms of generalized Hodgkin-Huxley models, the present work both classifies phenomena in terms of their generative mechanisms, and helps to define as structured data groups of phenomena that had heretofore seemed to be unrelated. We will develop the model in three stages and will indicate those data properties that can be explained at each stage. The first stage defines the basic gated pacemaker, whose properties already suffice to explain various circadian data. The second stage augments the gated pacemaker to include feedback generated by metabolic activity, which we think of as an index of fatigue. The analogous process in models of motivated behavior such as eating is a feedback signal due to satiety (Grossberg, 1982a, 1982b, 1982c). The third stage includes a slowly varying automatic gain control process. In models of motivated behavior, the analogous process describes how cues that are persistently associated with a motivated behavior become conditioned reinforcers that can thereupon modulate the activity cycle of that behavior. Our gain control process is not a "learning" process of the type that Pittendrigh and Daan (1976) criticized by saying (p. 248): "We see no utility in...treatment of circadian rhythms as being 'imprinted' on organisms...The structure of circadian pacemakers, including provision for some lability is completely encoded in DNA...". The gain control process is free from this criticism both because the basic gated pacemaker properties are independent of the gain control process and because all the processes in the model could be genetically specified.

The gated pacemaker model represents a single pacemaker system.

We have in mind the pacemakers that have been located in each of the two suprachiasmatic nuclei (SCN) of mammals (Moore, 1973, 1974; Moore-Ede, Sulzman, and Fuller, 1982). Various studies have indicated that these pacemakers drive the sleep, activity, feeding, and drinking cycles in mammals (Enright, 1980; Moore-Ede, Sulzman, and Fuller, 1982; Wever, 1979). In humans, the temperature cycle can be desynchronized from the sleep cycle, thereby suggesting that the temperature cycle is driven by a separate pacemaker system (Wever, 1979).

Recent models have focused on how these two distinct pacemaker systems are coupled (Enright, 1980; Kronauer, Czeisler, Pilato, Moore-Ede, and Weitzman, 1982; Wever, 1979). In these models, the individual pacemakers are chosen for convenience and simplicity, but do not admit a detailed physiological interpretation. For example, the Kronauer et al. (1982) and Wever (1962, 1975) models consist of a pair of coupled van der Pol equations. The model of Kawato and Suzuki (1980) consists of a pair of coupled FitzHugh-Nagumo equations. The more abstract model of Daan and Berde (1978) describes a pacemaker entirely in terms of its period, phase, and phase shifts. Our analysis complements these contributions on the coupling of formal oscillators by explicating the dynamics of a single pacemaker. Those results about coupled oscillators which are insensitive to the detailed properties of the individual oscillators will carry over to the case where gated feedback networks are the oscillators to be coupled.

We, however, argue that some properties which have heretofore been assumed to necessarily follow from the coupling between oscillators can be explained by internal properties of a single oscillator, notably rhythm splitting and long-term after-effects. This claim does not deny the existence of coupling between distinct sleep and temperature systems. Nor does it deny the existence of distinct pacemakers in each of the two suprachiasmatic nuclei of a mammal. Rather we show

how properties which cannot be explained without coupling between classical oscillators can be explained by a single gated oscillating system, and that some properties which have not been explained by coupling between classical oscillators can be explained by a single gated oscillator. At the very least, these results show that further argument is needed to conclude that a coupling between oscillators generates a data property when the individual oscillators are poorly characterized.

III.3. Some Circadian Phenomena and Gated Pacemaker Properties

This section summarizes some of our model's explanations of circadian data. A more complete exposition is contained in our other articles (Carpenter and Grossberg, 1982a, 1982b). In our analysis, certain circadian properties are attributed to the gated pacemaker. Other phenomena are understood as due either to metabolic feedback or to slow gain control. Some important properties, such as slowly evolving split rhythms, require the entire system. Each level of analysis provides specific predictions about the anatomy and physiology of the circadian system. Several of these predictions challenge prevailing assumptions in circadian models.

A) Competition Between On-Cells and Off-Cells

The basic model consists of on-cell/off-cell pairs, or dipoles, which mutually inhibit one another. The on-cell drives observable activity, such as wheel-turning. Light is hypothesized to influence the endogenous circadian cycle by differentially exciting the on-cells or off-cells of the dipole, depending on whether the model depicts a diurnal or nocturnal animal. These hypotheses are consistent with the observations that electrically stimulating the optic nerve, or stimulating the retina by light, excites some cells of the suprachiasmatic

nuclei while inhibiting others (Groos and Mason, 1978; Groos and Hendriks, 1979; Lincoln, Church, and Mason, 1975; Moore-Ede, Sulzman, and Fuller, 1982; Nishino, Koizumi, and Brooks, 1976). When these data are interpreted in terms of a van der Pol or other formal oscillator, an anatomical conclusion is drawn that differs from our own viewpoint in the following way.

B) Phase Resetting in Diurnal and Nocturnal Animals

In the gated pacemaker model, the assumption that light inputs excite the on-cells of diurnal animals and the off-cells of nocturnal animals leads to the expected day-activity of diurnal animals and night-activity of nocturnal animals. This assumption also implies that light resets the phase of both diurnal and nocturnal gated pacemaker models in a similar way, as demanded by the data (Pittendrigh, 1960, 1974).

For example, during the "early subjective night" of a model diurnal animal, a light pulse exciting the on-cell prolongs its active phase, delays the rest cycle, and thereby creates a phase delay. During the "early subjective night" of a model nocturnal animal, a light pulse exciting the off-cell prolongs its active phase, delays the ensuing activity cycle, and again creates a phase delay. During the "late subjective night" of a diurnal animal, a light pulse exciting the on-cell induces a premature onset of on-cell activity, thereby causing a phase advance in the onset of activity. During the "late subjective night" of a nocturnal model animal, a light pulse exciting the off-cell induces a premature onset of off-cell activity, thereby causing a phase advance in the onset of rest which, in turn, causes a phase advance in the onset of activity. For both diurnal and nocturnal model animals, a light pulse during the "subjective day" has little effect. Thus the characteristic phase response curves of both di-

urnal and nocturnal model animals are similar, as also occurs in vivo. Thus if a gated pacemaker exists in the SCN, then the phase response curves of both diurnal and nocturnal animals can be explained by SCN dynamics.

By contrast, if a van der Pol oscillator is used to model the pacemaker, then it is difficult to see how the diurnal/nocturnal distinction could be built in until after the SCN level, as Moore-Ede et al (1982, p.81-82) realized: "The circadian systems of diurnal and nocturnal species must be organized differently to account for the dramatic differences in the phase relationships of their rhythms to the light-dark cycle [i.e., day-active vs. night-active]. It is possible that the differences lie in the coupling between zeitgeber and pacemaker. However...the similarities between nocturnal and diurnal species in the way that light resets circadian pacemakers [i.e., the phase response curves] make it more likely that the difference in the phase relationships of the rhythms of nocturnal and diurnal animals actually depends on differences in the coupling mechanisms between the circadian pacemaker and the rhythms it drives."

If the transmitter gates which our model hypothesizes to exist in the SCN could be parametrically excited or inhibited during phase resetting experiments, then predictable changes in the phase response curves would be generated that could not be explained by a formal oscillator model.

C) Suppression of Circadian Rhythm by Steady Bright Light

Another property of a gated pacemaker that is often not discussed in formal models of coupled oscillators concerns the parametric response to increases in a steady background light level. Aschoff (1979, p.238) writes: "At high intensities of illumination circadian systems often seem to break down, as primarily exemplified by arhythmicity in

records of locomotor activity. Data supporting this statement have not often been published but the phenomenon is familiar to everyone working in the field."

In a gated pacemaker, sufficiently high steady light quenches the circadian rhythm. Activity is then determined by competition between motivated behaviors that are modulated by aperiodic environmental cues.

D) Period Doubling and Biorhythms

When humans live in caves for long periods in dim steady light, their circadian rhythm occasionally drifts towards a forty-eight hour day (Jouvet, Mouret, Chouvet, and Siffre, 1974). A period doubling phenomenon can also occur in the basic gated pacemaker model without light input. A normal period is achieved using the same choice of parameters in response to periodic light. Slow modulations of activity on a time scale much longer than a day can also occur. These phenomena are described in greater detail in Section III.6.

E) Split Rhythms and Metabolic Feedback

Pittendrigh (1960) first noted, and recognized the importance of, the phenomenon of split rhythms, whereby a nocturnal animal with a single daily activity cycle in the dark may generate an activity cycle which splits into two components in constant light. In recent years, numerous examples of split rhythms have been discovered. Hoffman (1971) described a diurnal animal (Tupaia belangeri) whose rhythm splits when the level of illumination is reduced; and Gwinner (1974) noted that the hormone testosterone induces split rhythms in starlings. Pittendrigh (1974) also noted that "Many animals tend to be bimodal in their activity pattern"(p.450) even when the activity pattern does not split.

Since Pittendrigh's original observations, many circadian models have adopted Pittendrigh's assumption that split rhythms are due to a pacemaker consisting of two or more coupled oscillators which drift out of phase when the split occurs:

"The circadian pacemaker for the activity cycle [a] comprises two separable oscillators, one responsible for the N [night, or earliest] component of a and the other for its M [morning, or later] component." (Pittendrigh, 1974, p.450).

"The findings reported here strongly suggest that the rhythms of locomotor activity in Tupaias is controlled by two coupled oscillators (or two groups of oscillators), which may have two stable phase relationships." (Hoffmann, 1971, p.142).

"Several recent investigations in mammals have made it virtually certain that the daily rhythm of gross locomotor activity...is governed by at least two coupled oscillators. This is strongly suggested by the observation that under certain conditions of constant illumination the rhythm of locomotor activity may 'split' into two distinct components..."(Gwinner, 1974, p.72).

"...Most of the behaviour of the rhythms observed may also be interpreted as complex responses of a single basic oscillator...The most compelling evidence for a two-oscillator system in vertebrates is the occurrence of 'splitting' of free-running activity rhythms into two distinct components." (Daan and Berde, 1978, p.298).

"...only a multi-oscillator arrangement could account for all the various behaviors of the mammalian timing system...Splitting of the activity pattern of rodents (Pittendrigh, 1960) was one of the earliest indications of multiple, potentially independent oscillators in mammals." (Moore-Ede, Sulzman, and Fuller, 1982, p.117-118).

We challenge the assumption that split rhythms necessarily imply the existence of in-phase/out-of-phase oscillators by explicitly demonstrating the existence of both split rhythms and bimodal activity patterns in a different type of model. At best, the traditional two-oscillator model now requires further proof.

In the gating model, split rhythms are caused by metabolic feedback due to activity. In this context, bimodal activity patterns are generated as follows: The pacemaker excites the on-cell and thereby

initiates activity, such as wheel-turning. Activity causes a build-up of metabolic feedback to the off-cell. This feedback enables the off-cell to partially inhibit the on-cell earlier than the on-cell transmitter gate's relatively large value would otherwise allow. Wheel-turning thereupon slows or ceases. The metabolic feedback has an opportunity to dissipate during this rest period. The on-cell is thereby disinhibited and its potential is revived by the still relatively large value of the on-cell transmitter gate. Activity thereupon increases until the combination of increased metabolic feedback and off-cell activation by the pacemaker bring on rest and sleep. For the same model animal, an environment that depresses on-cell potential, such as constant light in a nocturnal animal, turns the rest period into the full-fledged sleep period of the split rhythm.

Our explanation thus suggests that a nonspecific effect on the pacemaker, say due to substances in the bloodstream, can cause split rhythms. This explanation is consistent with electron microscopic evidence that some SCN cells are clustered in direct apposition to the walls of blood capillaries (Moore, Card, and Riley, 1980; Card, Riley, and Moore, 1980). As Moore-Ede et al. (1982) note, these cells "may act as receptors, sensing hormonal signals from elsewhere" (p.172). Indeed, it has been observed that injection of hormones can induce split rhythms (Gwinner, 1974). Our hypothesis is also supported by the fact the split rhythms are observed in higher organisms, although, in theory, it is possible for depletion of a chemical in a lower or unicellular organism to have a similar effect.

The metabolic feedback term in our model explicates the intuitive idea that activity per se, or other metabolically mediated processes, can influence our need to rest. The model also indicates how subtle the interaction between the underlying pacemaker and contingent activity can be. Because the metabolic feedback process rises and falls

in the model on an "ultradian" time scale that is significantly shorter than the 24-hour day, it helps to account for the approximately 6-, 8-, or 12-hour components of activity sometimes seen, for example, when a nocturnal animal is put in the dark after its circadian rhythmicity has been eliminated by leaving it in steady light (Pittendrigh, 1960, p.172).

F) Unilateral Lesions of the SCN Abolish Split Rhythms: The Internal Zeitgeber

When a nocturnal animal such as a golden hamster is maintained in constant light, a split rhythm can develop. Surgical ablation of one of the two SCN in the hamster eliminates the split rhythm (Pickard and Turek, 1982). The ablation also causes a total reduction in activity and a greater temporal diffuseness of activity.

These data imply that a functional relationship exists between the two SCN that helps to synchronize as well as to split the hamster's activity rhythm. The nature of this functional relationship requires close scrutiny. Pickard and Turek (1982) wrote that more than one interpretation is possible: "...the two SCN oscillators...might normally be coupled, but this coupling might be altered under...the split condition...Another possibility is that a set of interacting pacemakers may reside in each SCN, and the loss of the split rhythm may be a consequence of the total number of these oscillators destroyed; whether or not the destruction is unilateral may not be important" (p.1121). The former interpretation of two oscillators going out of phase due to a change in their mutual coupling is the more familiar one. To explain how removal of one SCN creates diffuse overall activity, this interpretation would need to suppose that several oscillators exist in each SCN and that, although the oscillators within either SCN do not mutually interact, the oscillators between the SCN do interact,

probably via an inhibitory coupling.

The gating pacemaker model explains both the abolition of the split as well as the reduction and diffuseness of subsequent activity without supposing that individual oscillators are differentially coupled within and between the two SCN. The model does this by explicating how a change in total activity causes the observed effects by reducing the metabolic feedback received by each cell in the remaining SCN. This explanation proceeds as follows.

Before an SCN is removed, every on-cell in each SCN contributes to a total excitatory signal that supports the observed activity level. (See function $G(x_1(t))$ in equation (65) of Section III.7). This total excitatory signal determines the total amount of metabolic feedback. Every off-cell in each SCN receives this <u>total</u> metabolic feedback signal. That is, the metabolic feedback signal is distributed <u>nonspecifically</u> to all the off-cells. In Section (E) above, we explained how this metabolic feedback signal can cause a split rhythm.

When one SCN is extirpated, the total number of on-cells that can generate activity is cut in half. Consequently, the total metabolic feedback signal to <u>each</u> surviving off-cell is soon also significantly reduced. This fact immediately indicates how the split rhythm is abolished, since in our model the split rhythm is ascribed to a relatively large metabolic feedback signal.

The diffuseness of activity is then explained in our model as it would be in a coupled SCN model. We assume that the remaining SCN contains several gated pacemakers which, in the absence of entraining signals, eventually get desynchronized. By contrast with a coupled SCN model, we suggest that the entraining signal may be received via the bloodstream; hence, its nonspecific character. To emphasize the fact that this metabolic feedback signal, which acts like a forcing function analogous to light, can be controlled by internal factors other

than the pacemakers themselves, we call it an internal zeitgeber.

G) Split Rhythm After-effects: Slow Gain Changes

When a nocturnal animal, such as a golden hamster, is placed in steady light, it may take a month or more for a split rhythm to evolve (Pittendrigh, 1974, p.449). In the present model, the slowness of the split onset is due to the action of a slow gain change that is analogous to the change in a cue's conditioned reinforcing efficacy in models of motivated behavior (Grossberg, 1982a, 1982b, 1982c). More precisely, the slow gain change is a process with two properties: its strength increases slowly as a function of on-cell activity; it acts as an excitatory signal to the on-cell that is proportional to its strength when the model animal is active. Otherwise expressed, the slowly varying gain process acts to gate an excitatory signal to the on-cell. This gating action is functionally distinct from the gating action that generates the underlying pacemaker oscillation.

Speaking intuituvely, the slowly varying gain signal causes the slow onset of the split as follows. A split rhythm is caused when metabolic feedback can get sufficiently large relative to the on-cell potential during an activity cycle. At the time when the model animal is placed in steady light, the slow gain signal is relatively large. It thereby enhances the on-cell potential during an activity cycle. After the model animal is placed in steady light, the light acts to excite the off-cell and thus tends to inhibit the on-cell. At first, the relatively large gain signal partially offsets this reduction in on-cell activity. Gradually, however, the gain signal senses the average reduction in the on-cell potential. The gain signal slowly decreases as a result, and the on-cell activity decreases further, on the average. As this progressive decrease in average on-cell activity proceeds, the metabolic signal gradually causes the rhythm to split.

When an animal whose rhythm is split is placed back into its original steady light environment, its rhythm can remain split indefinitely (Hoffmann, 1971). In our model, the split rhythm occurs when the gain signal is sufficiently small to allow metabolic feedback to split the on-cell activity cycle. Under certain circumstances, the average on-cell activity thereby decreases. When this occurs, the gain signal also tends to remain small. The splitting mechanism hereby tends to perpetuate itself unless a sufficiently potent and sustained counteracting influence is imposed, as Hoffmann (1971) also found.

Many authors interpret the slow onset and offset of split rhythms as a desynchronization phenomenon. In our theory, the slow onset and offset are attributed to the same mechanism that we use to explain after-effects, as in Section (I) below. In fact, our theory explains a variety of slowly varying processes using just this gain control mechanism. In particular, this mechanism has been used to numerically simulate several of the different types of split rhythms that are found in the data (Pittendrigh, 1974, p.449).

H) Aschoff's Rule and Its Exceptions: Paradoxical Results on After-effects

Additional support for the existence of a slow gain control process that reflects average activity comes from a correlative analysis of three types of data: Aschoff's rule and its exceptions, split rhythms in diurnal and nocturnal animals, and long-term after-effects on period subsequent to phase leads and lags caused by light pulses. In the experimental literature, no correlation has been drawn between these three types of phenomena. Our model rationalizes the split rhythm data using the mediating hypothesis that a slow decrease in the gain control signal tends to make split rhythms more likely, whereas a slow increase in the gain control signal tends to make split rhythms

less likely.

Aschoff's rule notes the tendency in many nocturnal mammals for an increase in steady light to cause an increase in period and a decrease in activity, and in some diurnal mammals for an increase in steady light to cause a decrease in period and an increase in activity (Aschoff, 1979). Exceptions to this rule frequently occur. In a different set of experiments, some diurnal mammals show split rhythms caused by an increase in light; others have rhythms which split in response to a decrease in light. Also, in some diurnal mammals, a transient lengthening of period during a phase shift is followed by a free-running rhythm of shortened period, whereas after a transient shortening of period, a lengthened free-running period is observed (Kramm, 1971). We correlate and unify such apparently unconnected observations using the properties of our gain control mechanism in another article of this series (Carpenter and Grossberg, 1982a).

I) Frequency After-effects

Pittendrigh (1974) wrote: "In our laboratory, we have found after-effects on the frequency of freerunning [in the dark] rhythms following: (1) phase shifts induced by light signals; (2) entrainment by cycles whose period is near the limit of entrainment...; (3) exposure to constant light; (4) change in photoperiod" (p. 441). Pittendrigh also noted that no mathematical model could yet explain these widespread phenomena. We have successfully simulated all of these phenomena using the slow gain control mechanism.

We will indicate below how the gain control mechanism generates one of these types of after-effects. In general, all of the cited manipulations which cause after-effects alter the total activity level, and thus the size of the gain signal in the model. The gain signal, and therefore the circadian period, may gradually return to its prior

level or may maintain a new level indefinitely, depending on the experiment.

An experiment in which photoperiod was manipulated will now be summarized (Pittendrigh, 1974, p.438). The photoperiod is the total duration of light within one circadian cycle. The experiment was done on a nocturnal rodent, the deermouse. First light was turned on periodically for one hour, followed by twenty-three hours of dark, for sixty days. Then the animal free-ran in the dark for thirty days. Next the animal was periodically exposed to eighteen hours of light followed by six hours of darkness for fifty days, after which the animal again free-ran in the dark until the end of the experiment. The total periods and activity levels during the two free-run intervals were different and maintained themselves for at least thirty days. The activity level after one-hour light pulses exceeded that after eighteen-hour light pulses. The period after one-hour light pulses also exceeded the period after eighteen-hour light pulses. Both of these effects were found in our numerical simulation despite the fact that the animal does not obey Aschoff's rule in this experiment.

The reason for the difference in activity levels is easily explained in terms of slow gain change. The difference in periods is due to a complex interaction that is not easily described in words. To see why free-running activity level decreases as light duration during the preceding photoperiods increases, note that an increase of light duration in a nocturnal animal causes a decrease in average on-cell activity, which in turn causes a gradual decrease in the gain signal. During the subsequent free-run interval, the smaller gain signal supports a smaller average level of on-cell activity. In all, an increase in light duration during the photoperiod causes a sustained decrease in activity during the subsequent free-run period.

III.4. The Gated Pacemaker

The gated pacemaker is described by a four-dimensional dynamical system, just as in the case of the Hodgkin-Huxley (1952) model. Whereas the Hodgkin-Huxley model contains one potential to which three auxiliary variables are coupled, the gated pacemaker model possesses two mutually interacting potentials to each of which is coupled a slow gating process. More precisely, the model describes interactions between two pairs of variables, (x_1,z_1) and (x_2,z_2). Each x_i is a "fast" variable that represents the voltage (or activity) of a cell (or cell population) v_i, i=1,2. Each z_i is a "slow" variable that represents the amount of stored transmitter in an excitatory feedback pathway from v_i to itself whose signals are gated by z_i, i=1,2. In particular, the z_i's correspond to the z variable in the gating model of Section II, equation (28).

The cell(s) v_1 is an on-cell and the cell(s) v_2 is an off-cell. Such on-cell/off-cell pairs, or dipoles, are widely found in the nervous system (Thompson, 1967). The on-cell and off-cell characteristics of v_1 and v_2 are due to the following constraints.

The potentials $x_1(t)$ and $x_2(t)$ mutually inhibit one another. The input J(t) which represents the (transduced) intensity of light excites the on-cell when the model represents a diurnal animal, but excites the off-cell when the model represents a nocturnal animal (Figure 18). In both diurnal and nocturnal model animals, the on-cell output energizes behavioral activity. Both the on-cell and the off-cell also receive an equal tonic input I that represents the arousal level of the dipole. Our model of the pacemaker in a suprachiasmatic nucleus consists of a family of these on-cell off-cell dipoles. Many of our results can be derived from the properties of a single such dipole.

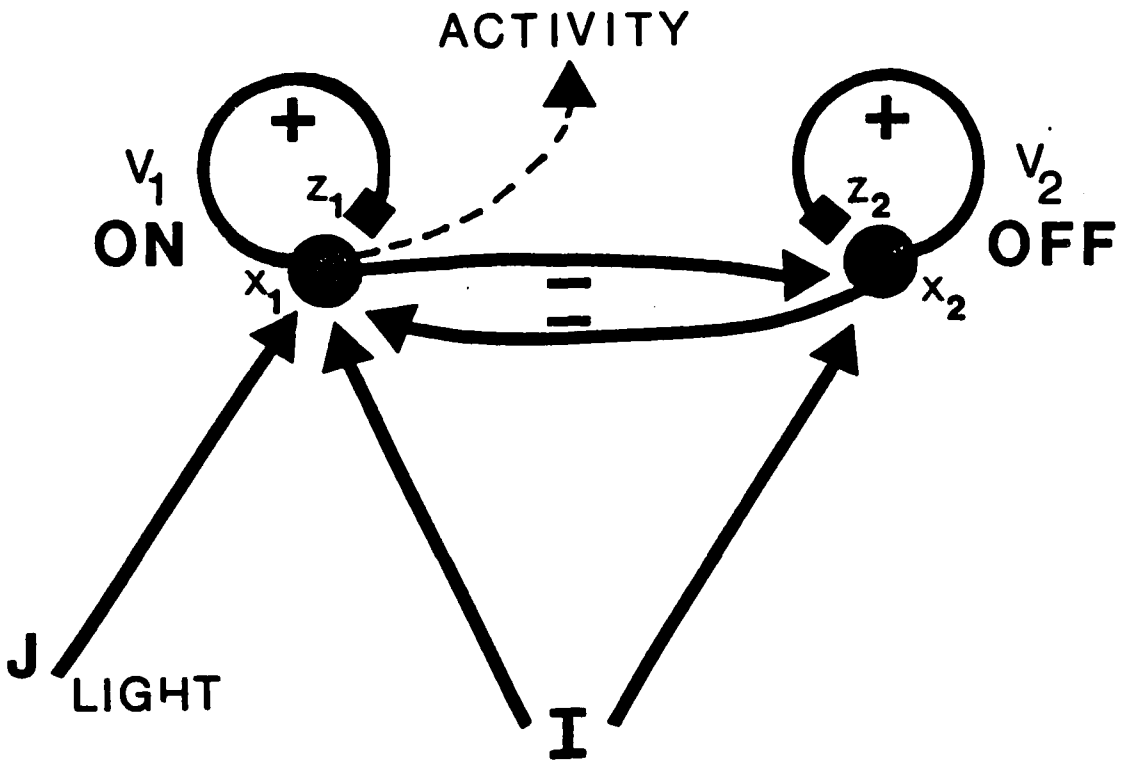

Figure 18: On-cell/off-cell anatomy with positive gated feedback and mutual inhibition. I is the tonic arousal input. J(t) represents the light input, which enters the on-cell in the diurnal model and which enters the off-cell in the nocturnal model.

The equations which describe the dynamics of the anatom, in Figure 18 are exactly analogous to the membrane equation (34) and the gating equation (28) from Section II:

$$C_0 \frac{dV}{dt} = (V^p - V)g^p + (V^+ - V)g^+ + (V^- - V)g^- \qquad (34)$$

and

$$\frac{dz}{dt} = A(B-z) - S(t)z. \qquad (28)$$

The on-cell and off-cell gating equations are thus

$$\frac{dz_1}{dt} = A(B-z_1) - f(x_1)z_1 \tag{52}$$

and

$$\frac{dz_2}{dt} = A(B-z_2) - f(x_2)z_2 \tag{53}$$

where $f(x_i)$ is proportional to the excitatory feedback signal transmitted by cell v_i, i=1,2. Our analysis considers signal functions of the form

i) Linear Above Threshold

$$f(w) = \begin{cases} w \text{ if } w > 0 \\ 0 \text{ if } w \leq 0 \end{cases} \tag{54}$$

or

ii) Sigmoid

$$f(w) = \begin{cases} \frac{w^2}{\alpha^2+w^2} & \text{if } w > 0 \\ 0 & \text{if } w \leq 0 \end{cases} . \tag{55}$$

The membrane equations for diurnal x_1 and x_2 are:

$$C_0 \frac{dx_1}{dt} = (x^p-x_1)g^p + (x^+-x_1)[I+J(t)+Cf(x_1)z_1] - (x^--x_1)Dg(x_2) \tag{56}$$

and

$$C_0 \frac{dx_2}{dt} = (x^p-x_2)g^p + (x^+-x_2)[I+Cf(x_2)z_2] - (x^--x_2)Dg(x_1) . \tag{57}$$

In (56) and (57), the constants x^p, x^+, and x^- are the passive, excitatory, and inhibitory saturation points, respectively. The excitatory conductance of x_1 is the sum of a tonic arousal input I, a light input J(t), and a positive gated feedback signal $Cf(x_1)z_1$. By contrast, the

excitatory conductance of x_2 does not contain a light input; in a model of a nocturnal animal, $J(t)$ is added to the excitatory conductance of x_2. The inhibitory conductance of x_1 is proportional to a feedback signal $g(x_2)$ from v_2. Typically $g(w)$ is chosen as in (54) or (55). The inhibitory conductance of x_2 is proportional to a feedback signal $g(x_1)$ from v_1. The two inhibitory conductances, taken together, express the mutual inhibition of v_1 and v_2.

Without loss of generality, we set $x^p = 0$ and put equations (52)-(57) in dimensionless form as follows:

$$\frac{dx_1}{dt} = -x_1 + (1-x_1)[C_1+J(t)+C_2 f(x_1)z_1] - (x_1+C_3)C_4 g(x_2) , \tag{58}$$

$$\frac{dx_2}{dt} = -x_2 + (1-x_2)[C_1+C_2 f(x_2)z_2] - (x_2+C_3)C_4 g(x_1) , \tag{59}$$

$$\frac{dz_1}{dt} = C_5(1 - z_1 - C_6 f(x_1)z_1) ; \tag{60}$$

and

$$\frac{dz_2}{dt} = C_5(1 - z_2 - C_6 f(x_2)z_2) , \tag{61}$$

where $C_1,\ldots,C_6$ are positive dimensionless constants; $x_1(t)$ and $x_2(t)$ are dimensionless variables which remain between $-C_3$ and 1; and $z_1(t)$ and $z_2(t)$ are dimensionless variables which remain between 0 and 1. Note that if the light input $J(t)$ is identically zero, then the pairs of equations for (x_1,z_1) and (x_2,z_2) are symmetric.

Further commentary is needed to characterize the light input $J(t)$. We assume that when light is on and the model animal is awake, then $J(t)$ equals the experimentally controlled light intensity. If the model animal is asleep, then $J(t)$ equals a constant fraction of the experimentally controlled light intensity. The model animal goes to

sleep when the on-cell potential $x_1(t)$ is smaller than a prescribed constant. In terms of equations (65) and (68) below, we assume that the animal goes to sleep when $G(x_1(t)) \leq \theta C_9$ where $0 < \theta < 1$.

III.5. Genesis of Unforced Pacemaker Oscillations: Strength of Inhibitory Coupling

This section and the next consider some of the types of oscillations that can occur within an unforced gated pacemaker in the dark. In this situation, the light input $J \equiv 0$ in (58). Consequently equations (58) and (59) for x_1 and x_2 and equations (60) and (61) for z_1 and z_2 are symmetric, and could represent pacemaker activity of either a nocturnal or a diurnal animal. This section describes how oscillations depend on the strength of the inhibitory coupling constant C_4 in (58) and (59). The next section describes how oscillations depend on the choice of the threshold constant C_7 of the excitatory feedback function

$$f(w) = \begin{cases} \dfrac{w^2}{C_7^2+w^2} & \text{if } w > 0 \\ 0 & \text{if } w \leq 0 \end{cases} \tag{62}$$

when

$$g(w) = \begin{cases} w \text{ if } w > 0 \\ 0 \text{ if } w \leq 0 \end{cases} . \tag{63}$$

In both cases, the choices (62) and (63) of signal functions are made. Surprisingly, parametric changes in C_7 cause totally different oscillatory waveforms than do parametric changes in C_4.

Choosing $C_4 = 0$ decouples the two potentials x_1 and x_2. In all of our numerical studies, this choice forces all the variables to approach limits $x_1(\infty)$, $x_2(\infty)$, $z_1(\infty)$, and $z_2(\infty)$ such that

$$x_1(\infty) = x_2(\infty) \text{ and } z_1(\infty) = z_2(\infty). \tag{64}$$

Such limits are said to occur on the diagonal. If f(w) is chosen to be linear above threshold, as in (54), then it can be proved that this outcome is necessary. We have, moreover, not found any numerical examples that violate this outcome. Consequently, we can assert that decoupling the two potentials quenches unforced oscillations. This conclusion strongly distinguishes our pacemaker model from other models in the literature.

Figures 19-24 describe how the behavior of the unforced gated pacemaker changes due to parametric increases in the inhibitory coupling strength C_4. This parametric series shows just the behavior one might expect: for weak coupling (Figure 19), the limit is on the diagonal; as C_4 increases, a small amplitude periodic solution bifurcates from the critical point (Figure 20); further increases in C_4 cause the amplitude and the period of the periodic solution to increase (Figures 21 and 22); a still stronger coupling elicits a large amplitude relaxation oscillation (Figure 23); finally, a very strong coupling enables the cell (population) v_1 or v_2, whichever has the larger initial values, to win the competition (Figure 24). The oscillation is thereby quenched and a limit is approached off the diagonal. Thus in all nontrivial cases, the solution pairs $(x_1(t), z_1(t))$ and $(x_2(t), z_2(t))$ eventually become 180° out of phase.

In Figures 19-24, two types of graphical representation are used. The first type of representation depicts the 4-dimensional phase portrait by projecting both pairs (x_1,z_1) and (x_2,z_2) onto an (x,z) coordinate plane. Each state of the system is then represented by a pair of 2-dimensional points. The second representation plots the functions $x_1(t)$ and $z_1(t)$ for $t \geq 0$. Because the pairs (x_1,z_1) and (x_2,z_2) are eventually 180° out of phase, the plots of $x_2(t)$ and $z_2(t)$ can also be

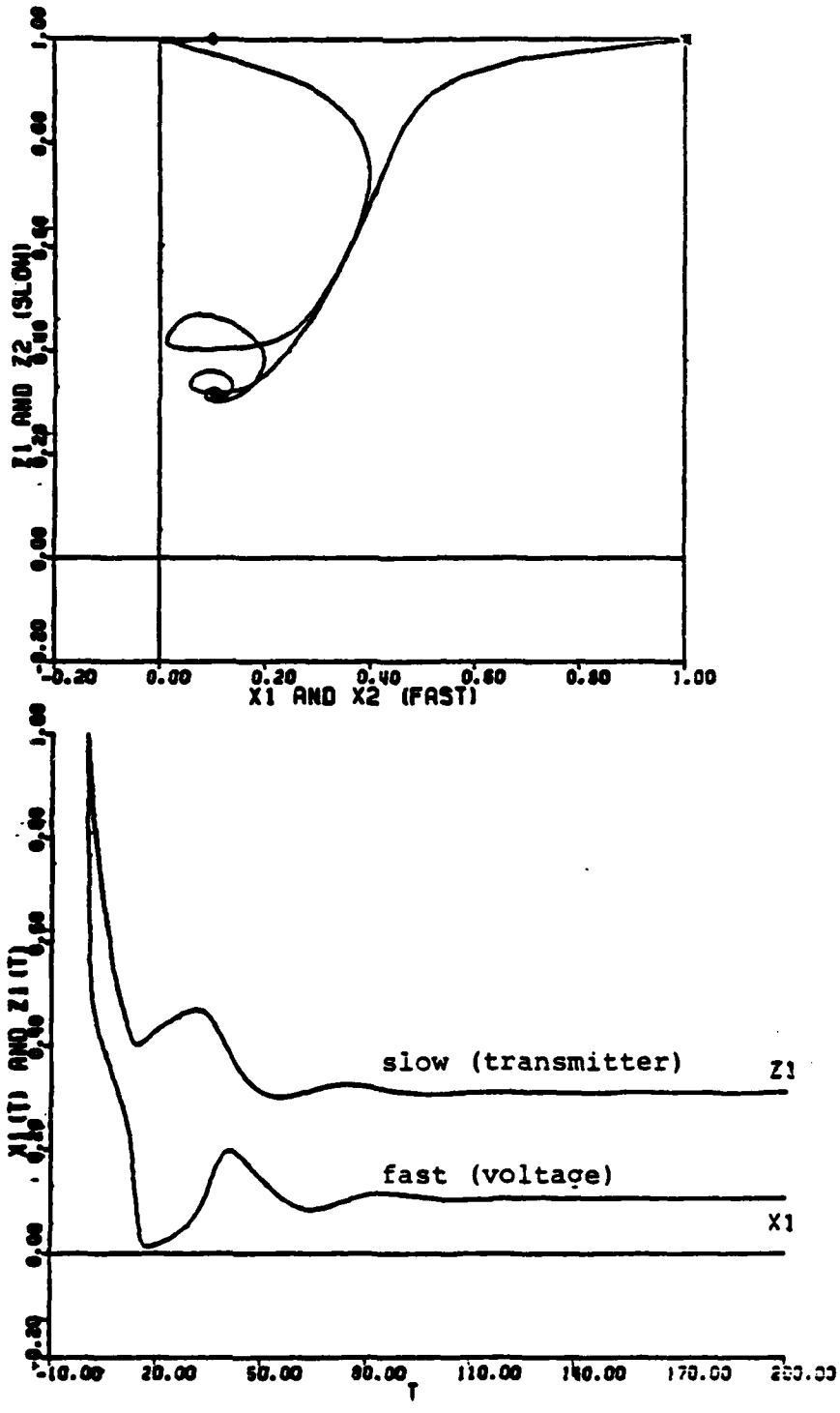

Figure 19: C_4 = 2. With weak inhibitory coupling, solutions go to a limit on the diagonal. In Figures 19-24, C_7 = .2 and C_4 varies.

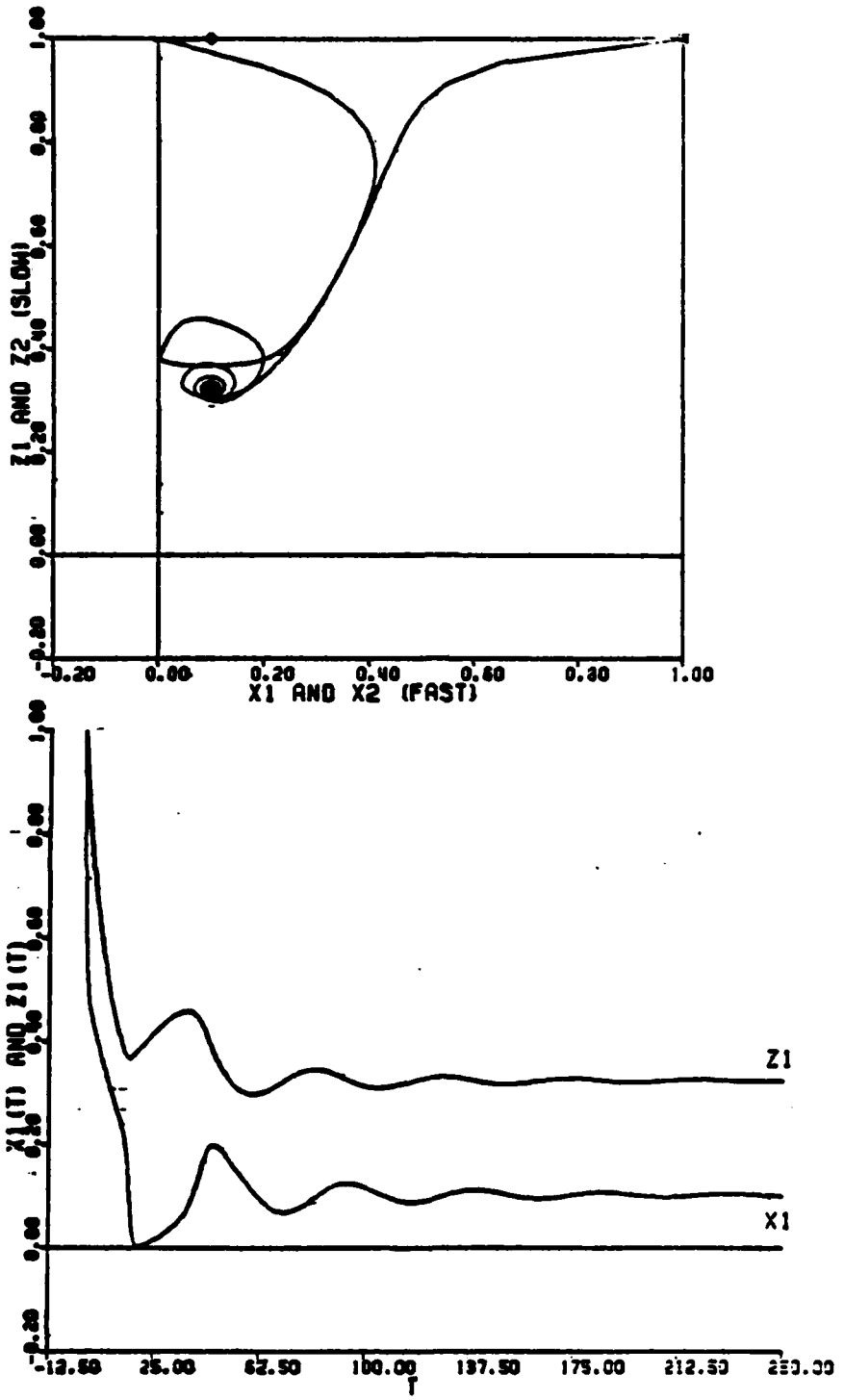

Figure 20: $C_4 = 2.3$. As coupling strength increases, a small amplitude periodic solution bifurcates from the critical point on the diagonal.

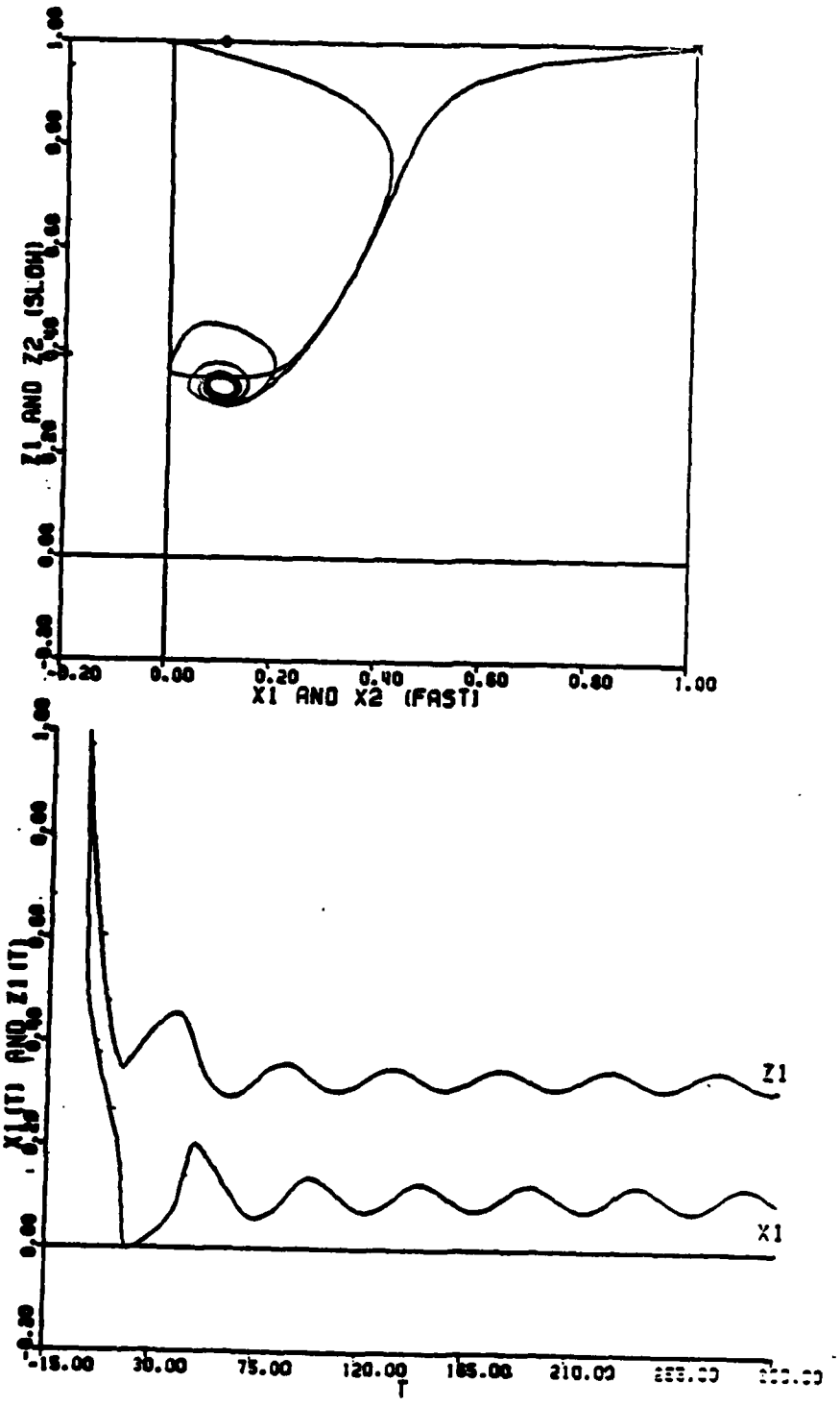

Figure 21: C_4 = 2.5. Amplitude and period increase.

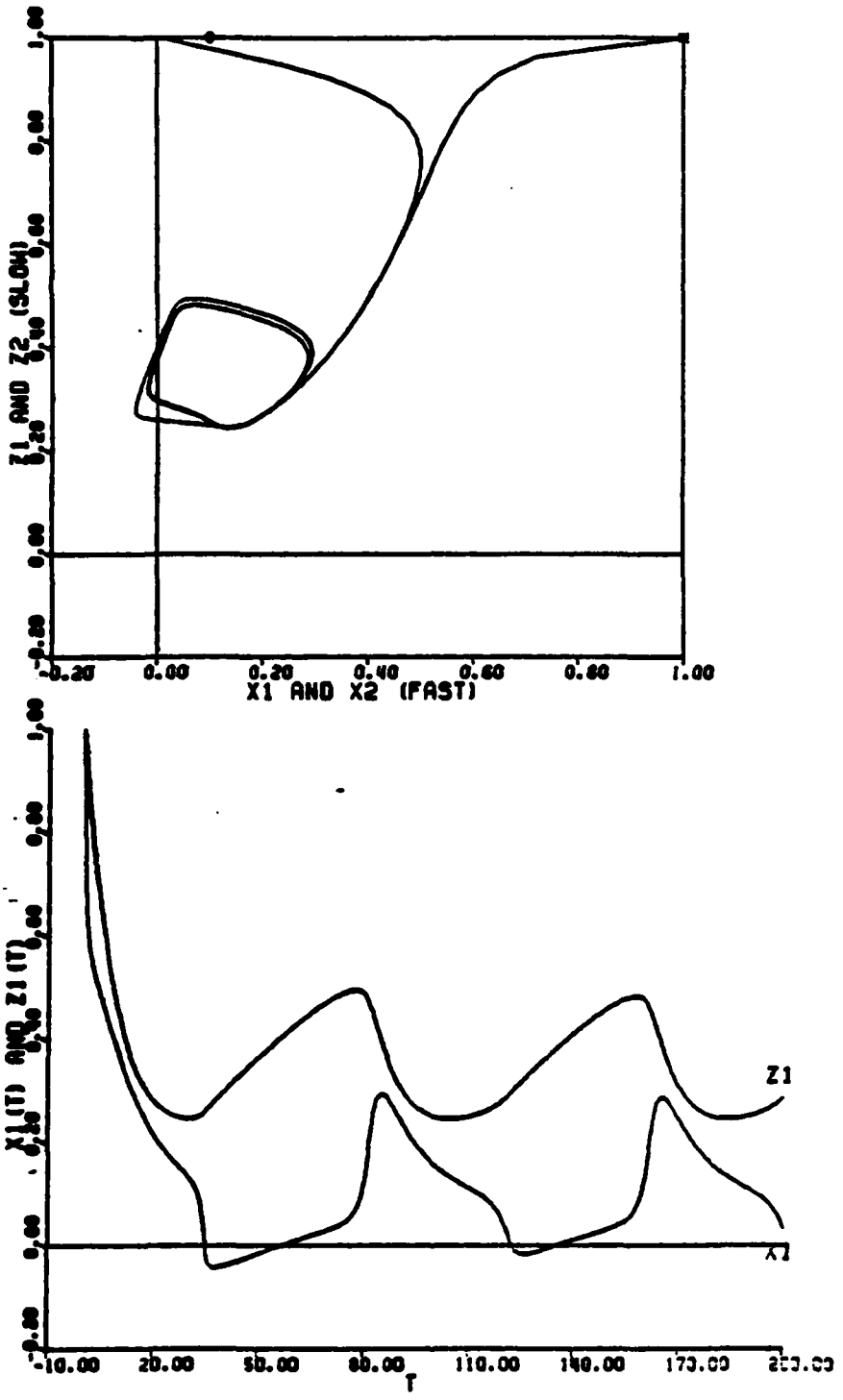

Figure 22: C_4 = 5. A large amplitude regular periodic solution.

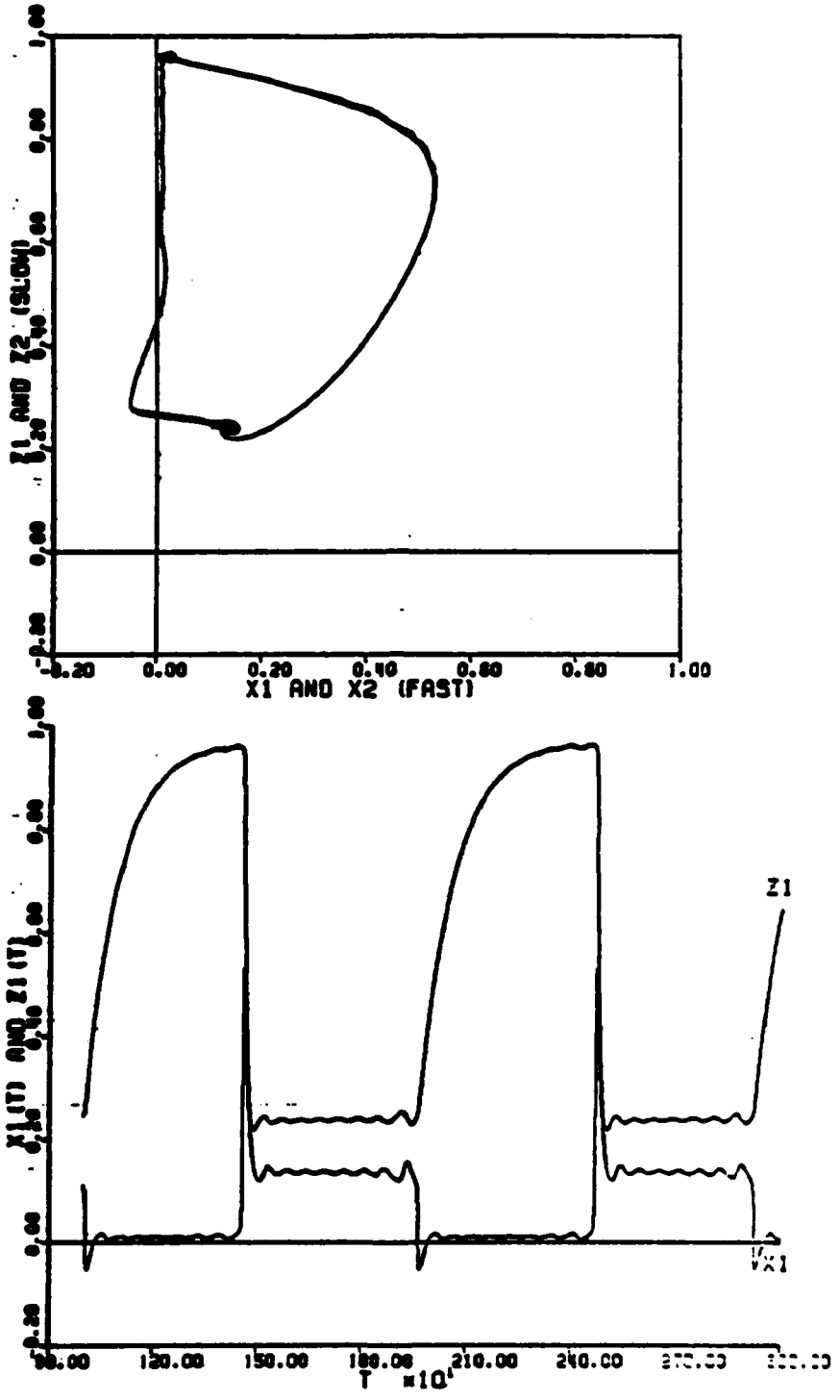

Figure 23: $C_4 = 6$. With strong inhibitory coupling, solutions oscillate near a plateau until there is a sudden switch, as if a tug-of-war is taking place.

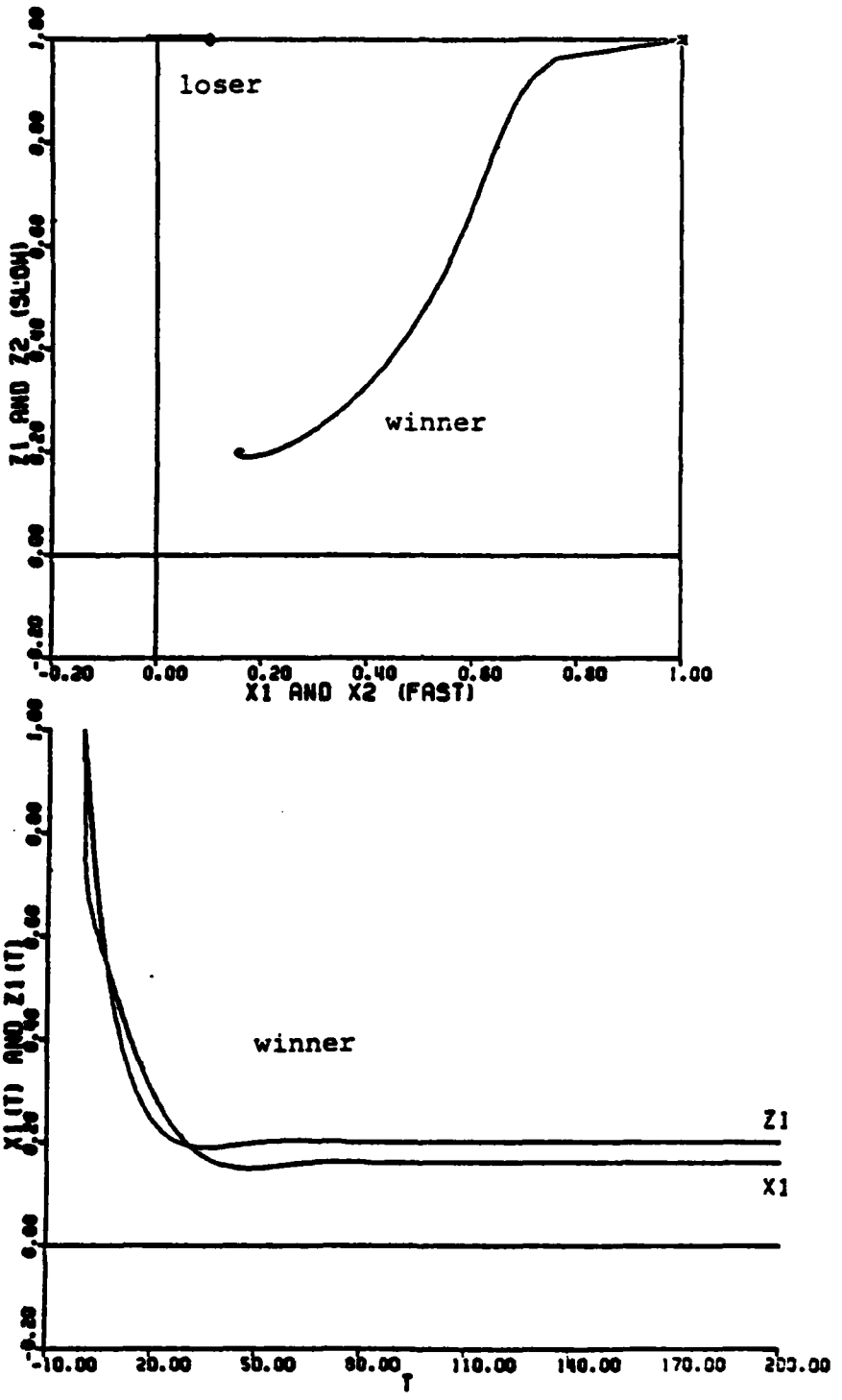

Figure 24: $C_4 = 7$. When inhibitory coupling is sufficiently strong, the pair (x_1, z_1) or (x_2, z_2) with the initial advantage wins the tug-of-war, and solutions go to a limit off the diagonal.

inferred.

The illustrated dynamics are robust over a wide range of parameters. Physical considerations have guided some constant parameter choices. For example, we let $C_3 = .1$ in (58) and (59) because C_3 is the ratio of V^- to V^+. In vivo, V^+ often stands for the saturation point of a Na^+ channel and V^- stands for the saturation point of a K^+ channel so that $V^+ >> V^-$. In the Hodgkin-Huxley (1952) model, for example, $C_3 \cong .1$. Also the "slow" rate C_5 of gate accumulation in (60) and (61) is chosen small relative to the "fast" unit rate of potential decay in (58) and (59). In particular, we choose $C_5 = .01$.

III.6. Period Doubling, Slowly Modulated Irregular Periodic Waves, and Chaos

Parametric changes in the signal threshold C_7 in (62) cause a dramatically different and novel sequence of oscillatory patterns. We start with the system illustrated in Figure 22. Here the choices $C_4 = 5$ and $C_7 = .2$ caused large-amplitude oscillations.

If C_7 is chosen very small, the signal function $f(w)$ in (62) makes a sharp jump from 0 to 1 as w increases. If C_7 is large, this signal function increases gradually from 0 to 1 as w increases. Given any choice of $C_7 > 0$, $f(C_7) = \frac{1}{2}$. In the parametric series in Figures 19-24, $C_7 = .2$, which is a moderate level because x_1 and x_2 can oscillate between -.1 and 1.

Figure 25 depicts the same system as Figure 22, but at large times. Consequently, the projected phase portrait looks like a single periodic solution, although really the two pairs (x_1,z_1) and (x_2,z_2) traverse this closed curve 180° out of phase. As C_7 increases from .2 to .35, an interval of C_7 values is reached wherein period doubling occurs (Figure 26). In other words, as C_7 is increased from .2 to .35, the regular periodic solution of Figure 25 is gradually deformed in

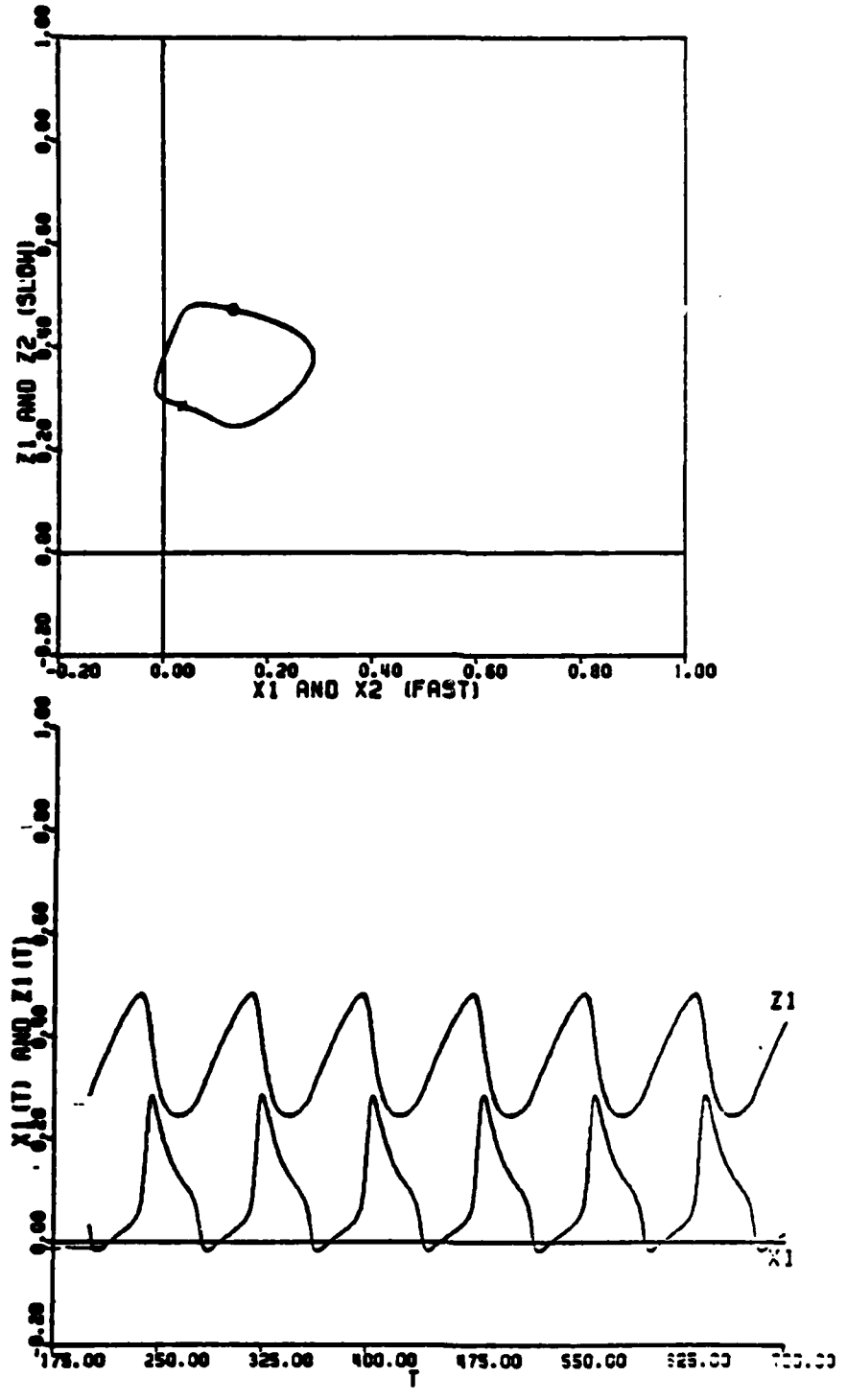

Figure 25: C_7 = .2. The large amplitude periodic solution of Figure 22, at later times. In Figures 25-29, C_4 = 5 and C_7 varies.

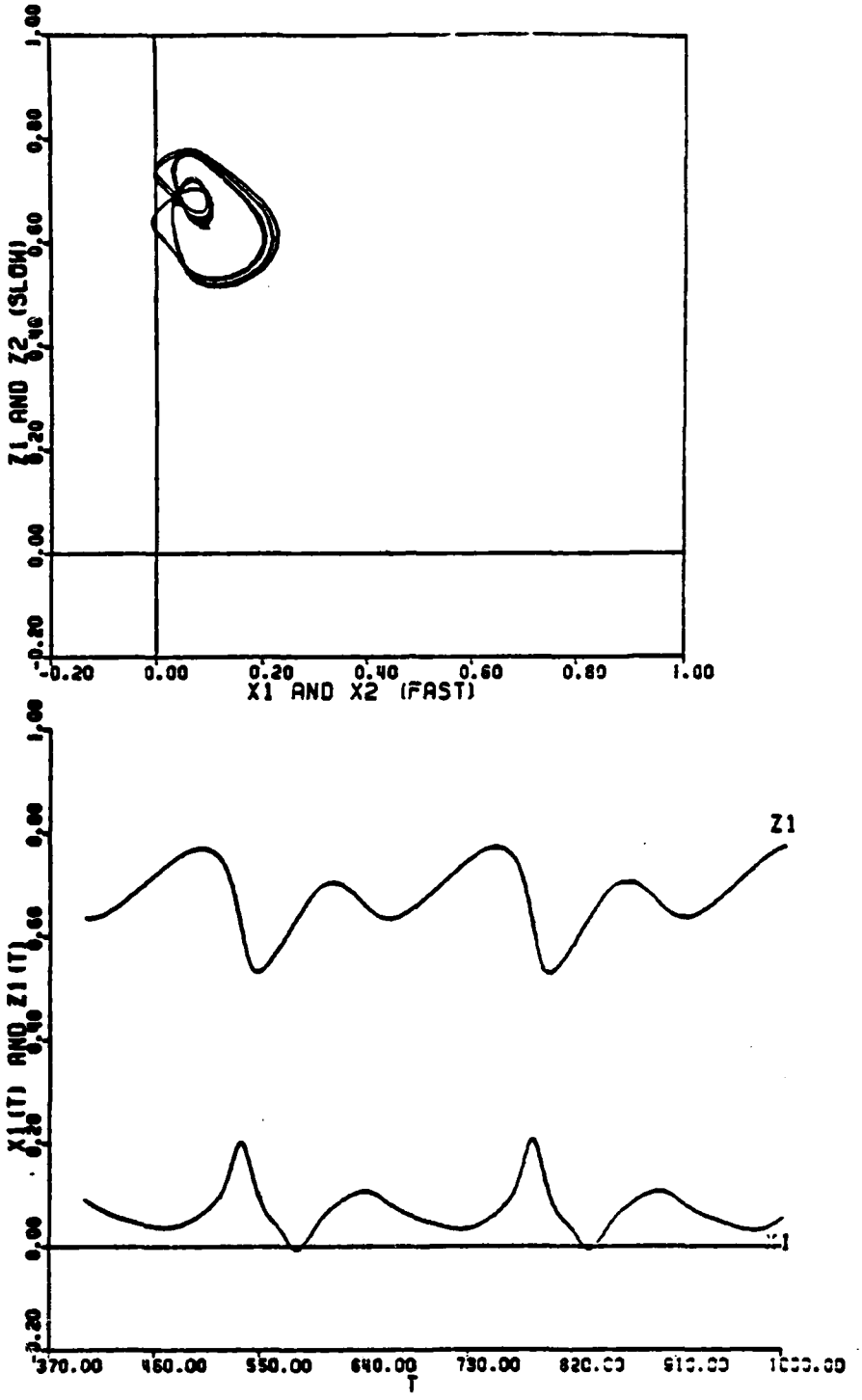

Figure 26: C_7 = .35. A period-doubled solution.

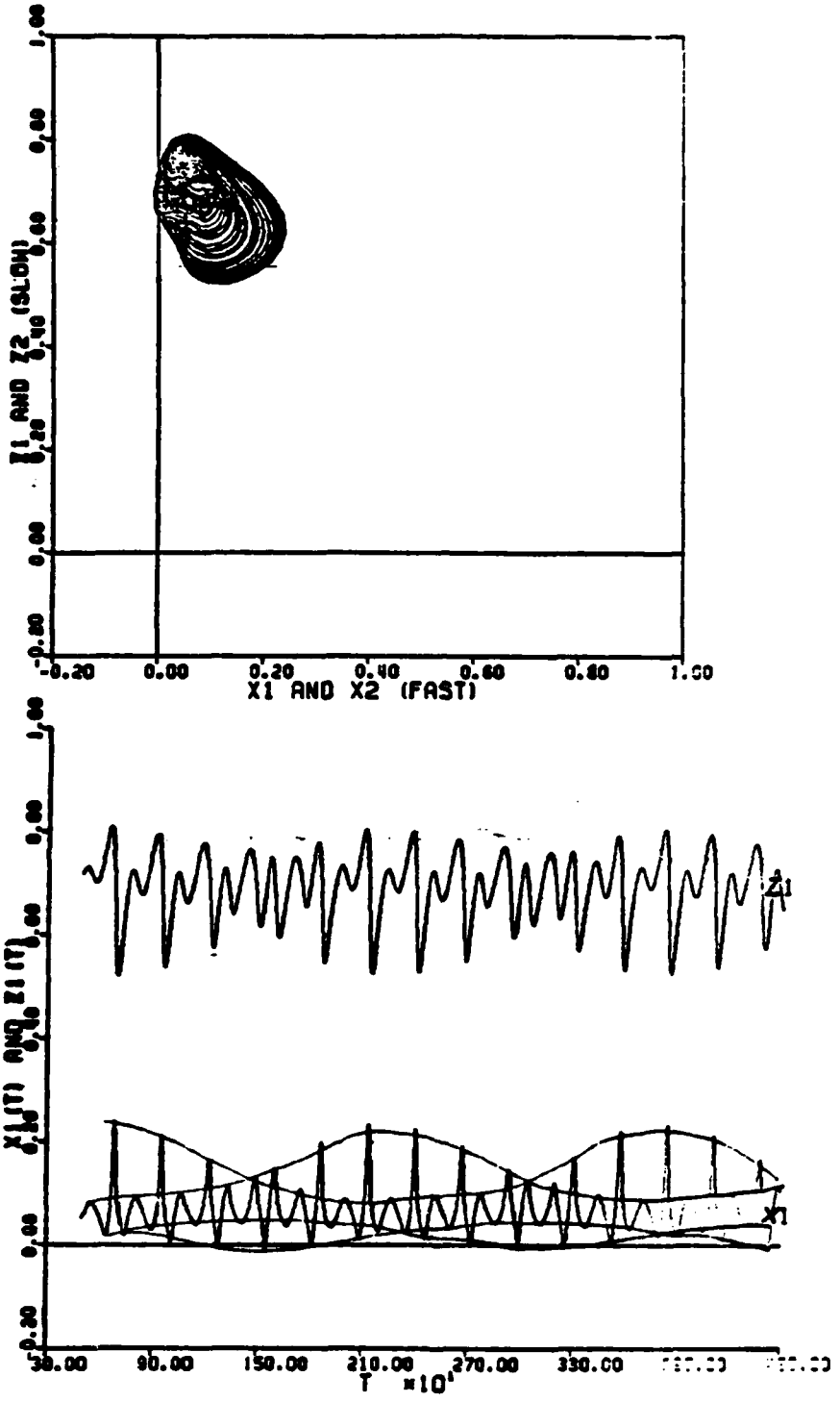

Figure 27: C_7 = .355. A slowly modulated period-doubled solution. The modulation is itself periodic.

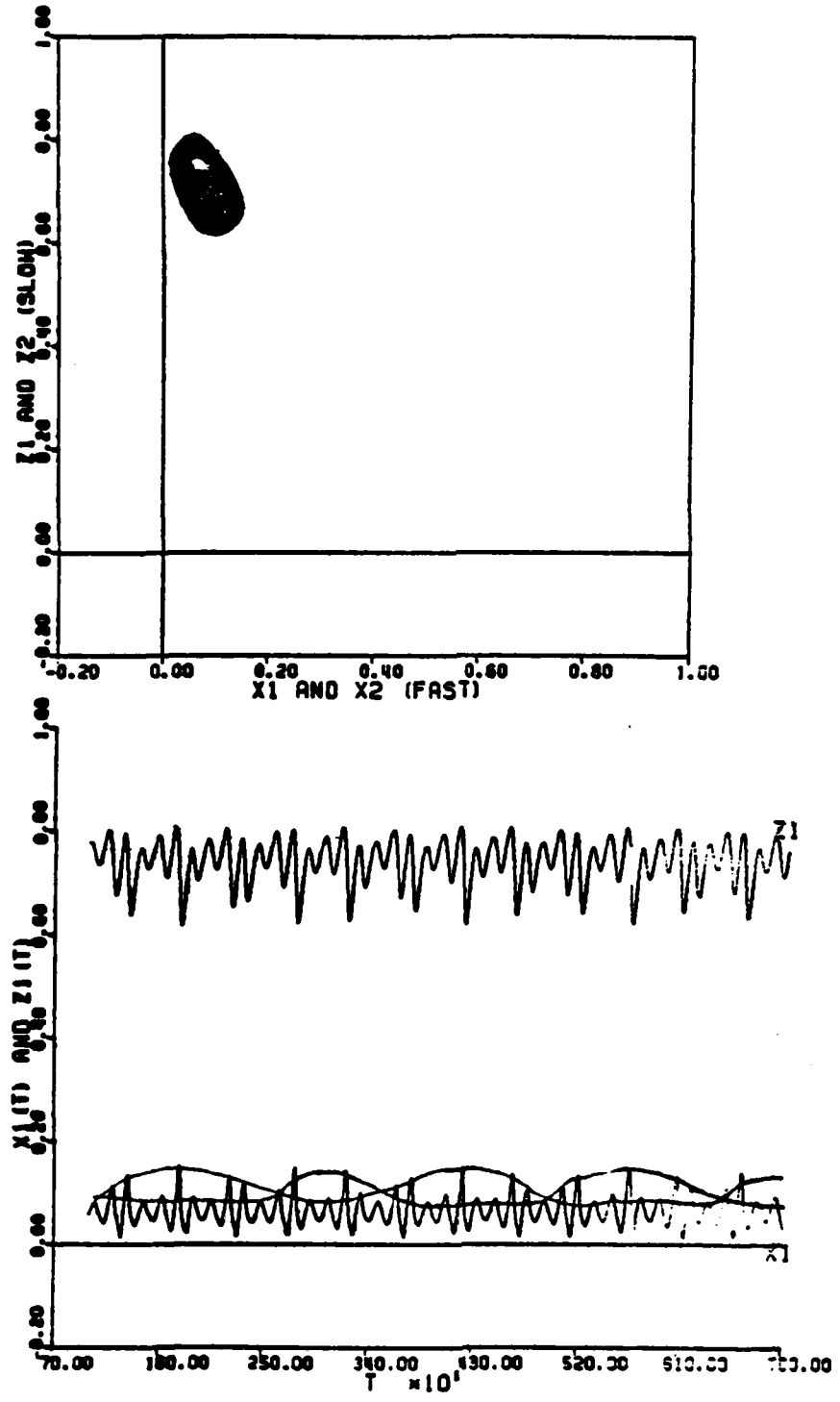

Figure 28: C_7 = .365. The period-doubled solution is modulated but with fewer oscillations per complete cycle and smaller amplitude than in Figure 27.

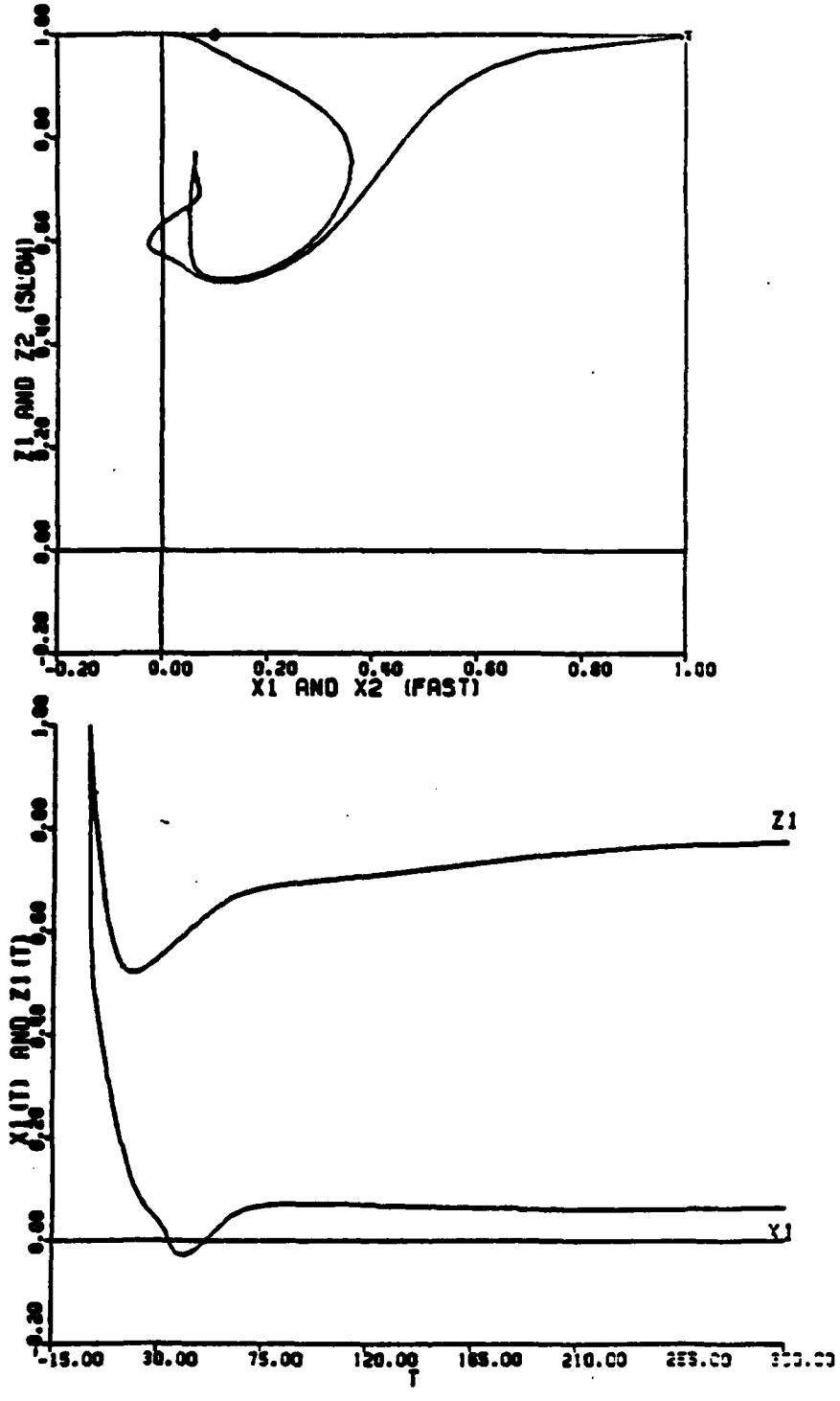

Figure 29: C_7 = .37. A small amplitude periodic solution near the diagonal.

such a way that every other peak gradually becomes smaller than its neighboring peaks. Consequently a period-doubled solution is a periodic solution in which a pair of large-then-small peaks repeats itself periodically through time. Thus, although a period-doubled solution is periodic it is not a regular periodic solution, due to the alternation in peak sizes. Such an irregular periodic solution is said to be period-doubled because at the transitional value of C_7 where the regular periodic solution becomes an irregular periodic solution, the period of the solution doubles.

A singular perturbation analysis has been developed to prove the existence of the regular periodic and period-doubled solutions as well as the transition between solutions (Carpenter and Grossberg, 1982b). This type of dynamic period doubling is different from the period doubling discovered by Feigenbaum (1978, 1979), which is currently a topic of great interest (Ruelle, 1981).

The existence of period-doubled solutions immediately suggests the possibility that chaotic solutions can also be generated by a gated pacemaker. Our numerical studies are insufficient to decide this issue, but we have observed a bifurcation of the period-doubled solutions to a new type of irregular periodic solution. In Figure 27, where $C_7 = .355$, the period-doubled amplitudes are slowly modulated on a time scale that is long compared to the interpeak duration. In terms of biological clocks, these slow modulations are suggestive of biorhythms and other slowly varying modulations of mood or activity level. In particular, if each peak represents a day, then the modulation in Figure 27 is on the order of magnitude of a month.

As C_7 increases to .365 (Figure 28) solution peaks are still slowly modulated, but all the peak amplitudes are smaller and there are fewer oscillations per cycle. When $C_7 = .37$ (Figure 29), the oscillations lie close to the diagonal. Finally, for sufficiently

large choices of C_7, the oscillations are quenched and the variables approach limits on the diagonal.

III.7. Metabolic Feedback and Slow Gain Control

The complete model is augmented with two types of slowly varying feedback. The feedback that measures activity-generated metabolic feedback is used to explain phenomena such as split rhythms, whereas the feedback due to slow gain control is used to explain phenomena such as long-term after-effects. Only the model of a diurnal animal will be considered herein. As before, the nocturnal model is identical except that J(t) appears in the x_2 instead of the x_1 conductance.

To define metabolic feedback, or fatigue, we suppose that the on-cell potential $x_1(t)$ generates a signal $G(x_1(t))$ that energizes observable activity, such as wheel-turning. We typically choose a sigmoid output function

$$G(w) = \begin{cases} \dfrac{w^2}{C_8^2+w^2} & \text{if } w > 0 \\ 0 & \text{if } w \leq 0 \end{cases} , \qquad (65)$$

and assume that the model animal becomes active if $G(x_1(t))$ exceeds a threshold C_9, and that suprathreshold activity is proportional to $G(x_1(t))-C_9$. We assume that a metabolic debt increases linearly with activity, and dissipates at a constant rate C_{10}. The metabolic feedback function is then

$$F(t) = C_{11} \int_0^t e^{-C_{10}(t-s)} \max[0, G(x_1(s))-C_9]ds . \qquad (66)$$

We assume that F(t) directly excites the off-cell(s) v_2 and thereby indirectly inhibits the on-cell(s) v_1 via competitive feedback. Equation (59) is then augmented to read

$$\frac{dx_2}{dt} = -x_2 + (1-x_2)[C_1+C_2 f(x_2) z_2+F] - (x_2+C_3)C_4 g(x_1) \quad . \qquad (67)$$

The metabolic feedback function F(t) generates a split rhythm as follows. The build-up of F(t) starts to inhibit the on-cell activity before it would otherwise be inhibited by the autonomous action of the pacemaker. The inhibition of on-cell activity, in turn, allows F(t) to dissipate, thereby disinhibiting the on-cell before the end of its usual on-phase. This explanation tacitly assumes that the gate $z_1(t)$ has not become too depleted during this time. A similar sequence of events helps to explain the bimodal frequency of activity that is often observed before rhythm splitting occurs (Pittendrigh, 1974, p.449).

The gain control process can be interpreted in several ways. It is formally the same as a model of how cues become conditioned reinforcers by being associated with the activity of drive representations (Grossberg, 1982a). In the present model, the on-cell v_1 plays the role of a drive representation. The conditioning process is formally equivalent to a slowly changing gain that is a long-term average of the on-cell activity level. The conditioning term hereby buffers the system against short-term fluctuations in light and acts as a stabilizing parametric change in response to pervasive alterations in light patterning, say due to seasonal changes.

The inputs that are gated by the gain control process have several alternative physical interpretations that have not yet been theoretically or experimentally tested. One interpretation is that the input is light itself. Another interpretation is that reinforcing cues, such as a wheel that has been turned, are the input sources. Finally, many circadian properties still obtain if the inputs are chosen to be constant. In all these cases, the slow gain changes can be used to formally explain all the types of long-term after-effects

on the frequency of the free-running circadian rhythms that were described by Pittendrigh (1974, p. 441).

For example, to represent an input that is turned on when the animal is awake we define

$$S(t) = \begin{cases} 1 \text{ if } G(x_1(t)) \geq \theta C_9 \\ 0 \text{ if } G(x_1(t)) < \theta C_9 \end{cases} . \tag{68}$$

The gain control function $y(t)$ is defined as a time-average of the product of input $S(t)$ times the on-cell activity $x_1(t)$. Thus

$$\frac{dy}{dt} = -C_{12}y + C_{13}Sx_1 . \tag{69}$$

The function $y(t)$ in turn gates the input $S(t)$ to create a net input to the on-cell v_1 that is proportional to $S(t)y(t)$, as in the following augmented equation for the on-cell potential:

$$\frac{dx_1}{dt} = -x_1 + (1-x_1)[C_1+J(t)+C_2f(x_1)z_1+Sy] - (x_1+C_3)C_4g(x_2) . \tag{70}$$

Note that two types of gating action occur in equation (70). Equations (60), (61), and (65)-(70) complete the definition of a gated pacemaker whose rhythm is modulated by both metabolic feedback and gain control feedback.

CONCLUSION

Three concepts persistently occur throughout this article. One is the classical concept that a membrane equation can model fast electrical responses in cells. The second is the concept that mass action processes can be coupled to the membrane equation as conductance terms. The third is the concept that gating processes can be used to model the mass action dynamics of chemical transmitters. Our use of these concepts illustrates how a small number of simple mechanisms can generate a wide diversity of complex biological phenomena, as well as parametric experimental tests of the models that simulate these phenomena.

REFERENCES

J. Aschoff, 1960, Exogenous and endogenous components in circadian rhythms, Cold Spring Harbor Symp. Quant. Biol. 25, 11-26.

J. Aschoff, 1979, Influences of internal and external factors on the period measured in constant conditions, Z. Tierpsychol. 49, 225-249.

J. Atkinson and A. Ward, 1964, Intracellular studies of cortical neurons in chronic epileptogenic foci in the monkey, Exp. Neurol. 10, 285-295.

J.L. Barker and T.G. Smith, Jr., 1978, Electrophysiological studies of molluscan neurons generating bursting pacemaker potential activity, in: Abnormal Neuronal Discharges (M. Boisson and N. Chalazonitis, Editors), Springer-Verlag, New York, 359-387.

D.A. Baylor and A.L. Hodgkin, 1973, Detection and resolution of visual stimuli by turtle photoreceptors, J. Physiol. 234, 163-198.

D.A. Baylor and A.L. Hodgkin, 1974, Changes in time scale and sensitivity in turtle photoreceptors, J. Physiol. 242, 729-758.

D.A. Baylor, A.L. Hodgkin, and T.D. Lamb, 1974a, The electrical response of turtle cones to flashes and steps of light, J. Physiol. 242, 685-727.

D.A. Baylor, A.L. Hodgkin, and T.D. Lamb, 1974b, Reconstruction of the electrical responses of turtle cones to flashes and steps of light, J. Physiol. 242, 759-791.

D.A. Baylor, T.D. Lamb, and K.-W. Yau, 1979, The membrane current of single rod outer segments, J. Physiol. 288, 589-611.

P.R. Benjamin, 1978, Endogenous and synaptic factors affecting the bursting of double spiking molluscan neurosecretory neurons (Yellow Cells of Lymnae Stagnalis), in: Abnormal Neuronal Discharges (M. Boisson and N. Chalazonitis, Editors), Springer-Verlag, New York, 205-216.

S.A. Binkley, 1979, A timekeeping enzyme in the pineal gland, Scientific American 240, 66-71.

W.H. Calvin, 1972, Synaptic potential summation and repetitive firing mechanisms: Input-output theory for the recruitment of neurons into epileptic bursting firing patterns, Brain Res. 39, 71-94.

J.P. Card, J.N. Riley, and R.Y. Moore, 1980, The suprachiasmatic hypothalamic nucleus: Ultrastructure of relations to optic chiasm, Neurosci. Abstr. 6, 758.

G.A. Carpenter, 1977a, A geometric approach to singular perturbation problems with applications to nerve impulse equations, J. Differential Equations 23, 335-367.

G.A. Carpenter, 1977b, Periodic solutions of nerve impulse equations, J. Math. Analysis and Appl. 58, 152-173.

G.A. Carpenter, 1979, Bursting phenomena in excitable membranes, SIAM J. Appl. Math. 36, 334-372.

G.A. Carpenter, 1981, Normal and abnormal signal patterns in nerve cells, in: Mathematical Psychology and Psychophysiology (S. Grossberg, Editor), SIAM-AMS Proceedings 13, 49-90.

G.A. Carpenter and S. Grossberg, 1981, Adaptation and transmitter gating in vertebrate photoreceptors, J. Theor. Neurobiol. 1, 1-42.

G.A. Carpenter and S. Grossberg, 1982a, Circadian rhythms, chemical transmitters, and motivated behavior, submitted for publication.

G.A. Carpenter and S. Grossberg, 1982b, A neural theory of circadian rhythms and related clocklike phenomena, submitted for publication.

S. Daan and C. Berde, 1978, Two coupled oscillators: Simulations of the circadian pacemaker in mammalian activity rhythms, J. Theor. Biol. 70, 297-313.

T. Deguchi, 1979, Circadian rhythm of serotonin N-acetyltransferase activity in organ culture of chicken pineal gland, Science 203, 1245-1247.

P.B. Detwiler, A.L. Hodgkin, and P.A. McNaughton, 1980, Temporal and spatial characteristics of the voltage response of rods in the retina of the snapping turtle, J. Physiol. 300, 213-250.

J.T. Enright, 1980, The Timing of Sleep and Wakefulness, Springer-Verlag, New York.

J.W. Evans, N. Fenichel, and J.A. Feroe, 1982, Double impulse solutions in nerve axon equations, SIAM J. Appl. Math. 42, 219-234.

D. Faber and M. Klee, 1972, Membrane characteristics of bursting pacemaker neurons in Aplysia, Nature 240, 29-31.

M.J. Feigenbaum, 1978, Quantitative universality for a class of nonlinear transformations, J. Statist. Phys. 19, 25-52.

M.J. Feigenbaum, 1979, The universal metric properties of nonlinear transformations, J. Statist. Phys. 21, 669-706.

J.A. Feroe, 1982, Existence and stability of multiple impulse solutions of a nerve equation, SIAM J. Appl. Math. 42, 235-246.

R. FitzHugh, 1961, Impulses and physiological states in theoretical models of nerve membrane, Biophysical J. 1, 445-466.

S. Grossberg, 1968, Some physiological and biochemical consequences of psychological postulates, Proc. Natl. Acad. Sci. 60, 758-765.

S. Grossberg, 1969, On the production and release of chemical transmitters and related topics in cellular control, J. Theor. Biol. 22, 325-364.

S. Grossberg, 1972a, A neural theory of punishment and avoidance, I. Qualitative theory, Math. Biosci. 15, 39-67.

S. Grossberg, 1972b, A neural theory of punishment and avoidance, II. Quantitative theory, Math. Biosci. 15, 253-285.

S. Grossberg, 1975, A neural model of attention, reinforcement, and discrimination learning, Inter. Rev. Neurobiol. 18, 263-327.

S. Grossberg, 1980, How does a brain build a cognitive code?, Psychol. Rev. 87, 1-51.

S. Grossberg, 1982a, The processing of expected and unexpected events during conditioning and attention: A psychophysiological theory, Psychol. Rev. 89, 529-572.

S. Grossberg, 1982b, Some psychophysiological and pharmacological correlates of a developmental, cognitive, and motivational theory, in: Cognition and Brain Activity (J. Cohen, R. Karrer, and P. Tueting, Editors), New York Academy of Sciences, New York.

S. Grossberg, 1982c, A psychophysiological theory of reinforcement, drive, motivation, and habit, J. Theor. Neurobiol., in press.

G.A. Groos and J. Hendriks, 1979, Regularly firing neurons in the rat suprachiasmatic nucleus, Experientia 35, 1597-1598.

G.A. Groos and R. Mason, 1978, Maintained discharge of rat suprachiasmatic neurons at different adaptation levels, Neurosci. Lett. 8, 59-64.

M.R. Guevara, L. Glass, and A. Shrier, 1981, Phase locking, period-doubling bifurcations, and irregular dynamics in periodically stimulated cardiac cells, Science 214, 1350-1353.

E. Gwinner, 1974, Testosterone induces "splitting" of circadian locomotor activity rhythms in birds, Science 185, 72-74.

S.P. Hastings, 1982, Single and multiple pulse waves for the FitzHugh-Nagumo equations, SIAM J. Appl. Math. 42, 247-260.

A.L. Hodgkin and A.F. Huxley, 1952, A quantitative description of membrane current and its application to conduction and excitation in nerve, J. Physiol. 117, 500-544.

K. Hoffmann, 1971, Splitting of the circadian rhythm as a function of light intensity, in: Biochronometry (M. Menaker, Editor), National Academy of Sciences, Washington, D.C., 134-150.

M. Jouvet, 1974, Monoaminergic regulation of the sleep-waking cycle in the cat, in: Circadian Oscillations and Organization in Nervous Systems (C.S. Pittendrigh, Editor), M.I.T. Press, Cambridge, Mass., 499-508.

M. Jouvet, J. Mouret, G. Chouvet, and M. Siffre, 1974, Toward a 48-hour day: Experimental bicircadian rhythm in man, in: Circadian Oscillations and Organization in Nervous Systems (C.S. Pittendrigh, Editor), M.I.T. Press, Cambridge, Mass., 491-497.

E. Kandel and W. Spencer, 1961, Electrophysiology of hippocampal neurons, II. After-potentials and repetitive firing, J. Neurophysiol. 24, 243-259.

M. Kawato and R. Suzuki, 1980, Two coupled neural oscillators as a model of the circadian pacemaker, J. Theor. Biol. 86, 547-575.

K.R. Kramm, 1971, Circadian activity in the antelope ground squirrel, Ammospermophilus leucurus, Ph.D. Thesis, Univ. of California, Irvine.

R.E. Kronauer, C.A. Czeisler, S.F. Pilato, M.C. Moore-Ede, and E.D. Weitzman, 1982, Mathematical model of the human circadian system with two interacting oscillators, Amer. J. Physiol. 242, R3-R17.

E. Lábos and E. Láng, 1978, On the behavior of snail (Helix pomatia) neurons in the presence of cocaine, in: Abnormal Neuronal Discharges (M. Boisson and N. Chalazonitis, Editors), Springer-Verlag, New York, 177-188.

A.J. Lewy, T.A. Wehr, F.K. Goodwin, D.A. Newsome, and S.P. Markey, 1980, Light suppresses melatonin secretion in humans, Science 210, 1267-1269.

T.-Y. Li and J.A. Yorke, 1975, Period three implies chaos, Amer. Math. Mon. 82, 985-992.

D.M. Lincoln, J. Church, and C.A. Mason, 1975, Electrophysiological activation of suprachiasmatic neurones by changes in retinal illumination, Acta Endocrinol. (suppl., Kbh.) 199, 184.

M. Markowitz, L. Rotkin, and J.F. Rosen, 1981, Circadian rhythms of blood minerals in humans, Science 213, 672-674.

R.M. May, 1976, Simple mathematical models with very complicated dynamics, Nature 261, 459-467.

H.P. McKean, Jr., 1970, Nagumo's equation, Adv. Math. 4, 209-223.

P.J. Mill, 1977, Ventilation motor mechanisms in the dragonfly and other insects, in: Identified Neurons and Behavior of Arthropods (G. Hoyle, Editor), Plenum Press, New York, 187-208.

R.Y. Moore, 1973, Retinohypothalamic projection in mammals: A comparative study, Brain Res. 49, 403-409.

R.Y. Moore, 1974, Visual pathways and the central neural control of diurnal rhythms, in: Circadian Oscillations and Organization in Nervous Systems (C.S. Pittendrigh, Editor), M.I.T. Press, Cambridge, Mass., 537-542.

R.Y. Moore, J.P. Card, and J.M. Riley, 1980, The suprachiasmatic hypothalamic nucleus: Neuronal ultrastructure, Neurosci. Abstr. 6, 758.

M.C. Moore-Ede, F.M. Sulzman, and C.A. Fuller, 1982, The Clocks That Time Us, Harvard University Press, Cambridge, Mass.

J. Nagumo, S. Arimoto, and S. Yoshizawa, 1962, An active pulse transmission line simulating nerve axon, Proceedings IEEE 50, 2061-2070.

E.J. Nestler, M. Zatz, and P. Greengard, 1982, A diurnal rhythm in pineal protein 1 content mediated by β-adrenergic neurotransmission, Science 217, 357-359.

H. Nishino, K. Koizumi, and C.M. Brooks, 1976, The role of suprachiasmatic nuclei of the hypothalamus in the production of circadian rhythm, Brain Res. 112, 45-59.

B.J. Nunn, G.G. Matthews, and D.A. Baylor, 1980, Comparison of voltage and current responses of retinal rod photoreceptors, Fed. Proc. 39, 2066.

P. Passouant and I. Oswald (Editors), 1979, Pharmacology of the States of Alertness, Pergamon Press, New York.

G.E. Pickard and F.W. Turek, 1982, Splitting of the circadian rhythm of activity is abolished by unilateral lesions of the suprachiasmatic nuclei, Science 215, 1119-1121.

C.S. Pittendrigh, 1960, Circadian rhythms and the circadian organization of living systems, Cold Spring Harbor Symp. Quant. Biol. 25, 159-182.

C.S. Pittendrigh, 1974, Circadian oscillations in cells and the circadian organization of multicellular systems, in: Circadian Oscillations and Organization in Nervous Systems (C.S. Pittendrigh, Editor), M.I.T. Press, Cambridge, Mass., 437-458.

C.S. Pittendrigh and S. Daan, 1976, A functional analysis of circadian pacemakers in nocturnal rodents, I. The stability and lability of spontaneous frequency, J. Comp. Physiol. 106, 223-252.

R.E. Plant and M. Kim, 1975, On the mechanism underlying bursting in the Aplysia abdominal ganglion R15 cell, Math Biosci. 26, 357-375.

J. Rinzel and J.B. Keller, 1973, Traveling wave solutions of a nerve conduction equation, Biophysical J. 13, 1313-1337.

F.A. Roberge, M. Gulrajani, H.H. Jasper, and P.A. Mathieu, 1978, Ionic mechanisms for rhythmic activity and bursting in nerve cells, in: Abnormal Neuronal Discharges (M. Boisson and N. Chalazonitis, Editors), Springer-Verlag, New York, 389-405.

D. Ruelle, 1981, Differentiable dynamical systems and the problem of turbulence, Bull. Amer. Math. Soc. 5, 29-42.

D.F. Russell and D.K. Hartline, 1978, Bursting neural networks: A reexamination, Science 200, 453-456.

J.S. Takahashi, H. Hamm, and M. Menaker, 1980, Circadian rhythms of melatonin release from individual superfused chicken pineal glands in vitro, Proc. Natl. Acad. Sci. USA 77, 2319-2322.

W.N. Tapp and F.A. Holloway, 1981, Phase shifting circadian rhythms produces retrograde amnesia, Science 211, 1056-1058.

R.F. Thompson, 1967, Foundations of Physiological Psychology, Harper and Row, New York.

A. Ward, Jr., 1969, The epileptic neuron: Chronic foci in animals and man, in: Basic Mechanisms of the Eplepsis, Little, Brown, and Company, Boston, 263-288.

T.A. Wehr and A. Wirz-Justice, 1982, Circadian rhythm mechanisms in affective illness and in antidepressant drug action, Pharmacopsychiat. 15, 30-38.

R. Wever, 1962, Zum Mechanismus der biologischen 24-Stunden-Periodik, Kybernetik 1, 139-154.

AD-A137 826 DYNAMIC MODELS OF NEURAL SYSTEMS: PROPAGATED SIGNALS PHOTORECEPTOR TRANDD..(U) BOSTON UNIV MA DEPT OF MATHEMATICS S GROSSBERG NOV 83 AFOSR-TR-84-0022 2/2

UNCLASSIFIED AFOSR-82-0148 F/G 6/16 NL

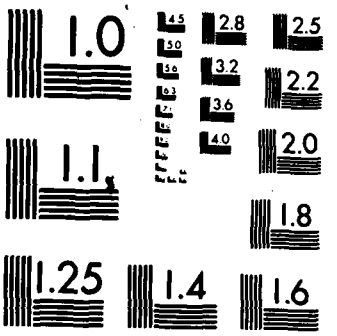

MICROCOPY RESOLUTION TEST CHART
NATIONAL BUREAU OF STANDARDS-1963-A

R. Wever, 1975, The circadian multi-oscillator system of man, Inter. J. Chronobiol. 3, 19-55.

R.A. Wever, 1979, The Circadian System of Man: Results of Experiments Under Temporal Isolation, Springer-Verlag, New York.

A.T. Winfree, 1980, The Geometry of Biological Time, Springer-Verlag, New York.

K.-W. Yau, P.A. McNaughton, and A.L. Hodgkin, 1981, Effect of ions on the light-sensitive current in retinal rods, Nature 292, 502-505.

M. Zatz and M.J. Brownstein, 1979, Intraventricular carbachol mimics the effect of light on the circadian rhythm in the rat pineal gland, Science 203, 358-361.

END

FILMED

3-84

DTIC